TU Delft

Biomechanical model to optimize unilateral blade running

Araceli Luque Martín-Sacristán

Biomechanical model to optimize unilateral blade running

by

Araceli Luque Martín-Sacristán

to obtain the degree of Master of Science in Biomedical Engineering
at the Delft University of Technology,
to be defended publicly on Monday April 12, 2021 at 9:00 AM.

Student number:	4901657	
Project duration:	May 4, 2020 – April 12, 2021	
Committee:	Dr. Frans van der Helm (daily supervisor)	TU Delft
	Thomas Geijtenbeek (daily supervisor)	TU Delft
	Otto Bergsma (chair)	TU Delft

Delft
University of
Technology

Contents

Abstract

Paralympic sports are growing more popular. Besides the dedicated training of the athlete, technology is crucial to empower amputees to perform at their highest level. The recent carbon fibre Running-Specific-Prosthesis (RSP) have energy stored and return capabilities that allow runners with amputations to perform almost as able-bodied. However, due to the difference in power output between a biological ankle and a RSP, unilateral transtibial (UTT) amputees need to adjust their biomechanics to an asymmetric pattern. It is known that the stiffness of the blade has a great influence on the performance of the athlete. The main challenge was to find a method to prescribe the optimal stiffness for a particular athlete, that allows him/her to perform the best in a race. The current approach to advice a RSP is based on the bodyweight of the athlete and the coaches and athletes wishes. Nevertheless, as a result of the insufficient number of subjects and the difficulty to perform a randomised control trial, there is limited evidence about the UTT athlete capability of adapting their muscle activity to different prosthesis stiffness and the optimal RSP stiffness for them.

In order to investigate this, two main **goals** for this master thesis project were raised: to implement a musculoskeletal model of an UTT amputee athlete wearing a RSP and predict its optimal running biomechanics through predictive forward dynamic simulations; to find the optimal athlete-RSP stiffness combination that maximizes the running performance. Five different stiffness of a Flex-Run Össur (Reykjavík, Island) RSP were modelled and simulated for the maximum velocity the model could reach.

Results: firstly, the model could perform better with a middle-class RSP category. It enhanced the hip muscles to exert more power in the blade during the first part of the stance phase. However, the prosthetic leg generated 41.2% lower total average power, including the RSP power, than the intact leg. The RSP made up 24.8% of the total prosthetic leg power. Secondly, the intact leg benefited from an improved push-off of the prosthetic leg having a favourable landing that allowed to exert more power and propel the body into longer flight time than with low-class RSP categories. Still, the top speed of the model was far from what athlete can achieve, but the motion and kinetic data were comparable for low running speeds.

Therefore, it could be concluded that a reasonable prediction of the optimal RSP stiffness for running at about 4.6 m/s was achieved. The presented biomechanical model could potentially be used to assist coaches and athletes to have a better idea of the most suitable RSP stiffness.

Preface

This master thesis project concludes my Master of Science in Biomedical Engineering studies at the Delft University of Technology in Delft, The Netherlands. This work was developed within the Research department of Biomechanical Engineering of TU Delft, in close collaboration with the Netherlands' Paralympic team.

I would like to thank everyone who has been there for me during this period of my life. First, I would like to express my acknowledgement to my supervisors. To Frans van der Helm, who gave me the opportunity to work on this exciting and challenging topic and believed in my capabilities. To Thomas Geijtenbeek, who was always there to answer my questions and provided valuable feedback when I was struggling.

Thank you to my friends from Delft. To Henar, for being like a sister in a foreign country and balancing my weaknesses. To Giorgio, for being a great fake housemate and sharing our battle against the Thesis. To Mo, for being always there and taking care of me. To Pingonas, for bringing the pingoneo and joy in a pandemic situation. To Giuseppe, who made me discover Latin dances in a cold country. To Uri and Javi for being the perfect housemates. To Álvaro, Jacob, Edamamens, compiamigos, paninis, and Stay Homas.

Last but not least, I would like to thanks my family. They were constantly supporting me in my worst moments. Especially to my mum, who encouraged me to come to Delft, boosted me every time I did not believe in myself and lived my triumphs as they were her own; this one is also yours.

To all of you, I sincerely thank you.

Araceli Luque Martín-Sacristán
Delft, April 2021

Introduction

According to the global leader orthopaedics company, Össur (Reykjavík, Island) [1], there are more than 750.000 new lower limb amputees worldwide each year. The statistics remark that 70% of amputees lose their limb due to vascular-related diseases or diabetes, 20% due to trauma and 10% because of other causes. From these new amputee group, the average age is about 65 years old, which is not quite active population, and only 30 to 40 % are fitted with prosthetic solutions. However, it is seen that the numbers differ between countries. For instance, United State has a relatively young amputee population, as a large number of amputations are war soldiers. The most common amputation is unilateral transtibial (UTT), making up 45 % of the total number of amputations (see, Figure 1).

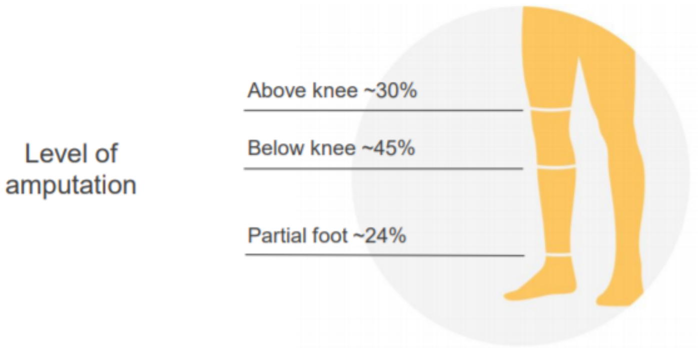

Figure 1: Level of amputations and their percentage among the amputee population [1].

Limb amputation causes negative effects not only on the physical well-being because of the lack of mobility, but also on mental health. Participation in sport is proven to be beneficial for these areas. Thereby, it is essential to encourage amputees to have an active life through the development of functional prostheses. Prostheses have been developed considerably since 1976 when amputee athletes wearing prostheses took part in the sprint event at the Paralympic Games for the first time. The complete revolution of lower-limb prostheses occurred when carbon composite material arrived at the prosthesis industry. Currently, carbon fibre prostheses are mainly used in elite sports.

Paralympic sports are growing more popular. Besides the dedicated training of the athlete, technology is crucial to empower amputees to perform at their highest level. The recent carbon fibre running prostheses have energy stored and return capabilities that have allowed runners with amputations to perform almost as able-bodied. However, there is still a great difference in sprinting times between them. The able body Usain Bolt set the world record to 9.58 seconds in 100 metres sprint, against the bilateral amputee Alan Oliveira and the UTT amputee Richard Browne who achieved 10.57 and 10.75 seconds respectively [15] [12]. Similar time differences also occur in the female category.

In particular, UTT amputees have longer sprinting times than bilateral amputees and able-bodied. This might be caused due to their dissimilarity in muscle mass distribution between legs. Due to missing the ankle joint in one leg, muscle power between legs is expected to be different. It has been shown that to compensate for this asymmetry, UTT amputees need to adjust their running pattern. Asymmetry between legs is found in terms of kinematics [25] , spatiotemporal variables [5] and Ground-Reaction-Forces (GRF) [3] [28] in UTT amputees. Nevertheless, these biomechanical adaptations are not well investigated. There is limited evidence of if this apparent disadvantage of UTT amputees over able-bodied and bilateral ones is due to their impairment and asymmetry between legs or to the athlete strength capability. This is a result of the lack of researches on this topic and the limited number of amputee subjects, which does not allow to perform a randomised controlled trial study. For this reason, the current studies have poor methodologies.

Furthermore, prosthesis design plays an important role in running performance for the amputee group. It is known that among other mechanical properties, prosthesis stiffness governs the dynamic behaviour of the running blade and it has a great influence on performance. Therefore, finding the optimal prosthesis stiffness for a specific athlete becomes very important to accomplish their best possible time in a race. However, the literature is not conclusive in which prosthesis setup is more optimal for UTT athletes. Moreover, there is no concern about the athlete capability of adapting their biomechanics to different prosthesis stiffness. This is because there is no current way of measuring the prosthesis behaviour while running in the field, and the difficulty of experimenting with different type of prostheses in the same study. For this reason, the choice of the prosthesis is currently to the wishes of the coaches and athletes themselves.

Coaches and athletes are looking for a method to prescribe the most suitable prosthesis for an athlete. Finding the optimal athlete-prosthesis stiffness combination as well as gaining more knowledge about the biomechanical adaptations of a UTT amputee is key to improve an athlete´s performance. A satisfactory approach to investigate this is using musculoskeletal models. Predictive forward dynamic simulations enable to emulate running motion for a musculoskeletal model with promising results. **The first goal of this project was to build a musculoskeletal model of a UTT amputee athlete, running with a running-specific-prosthesis in order to investigate their optimal asymmetric motion pattern. The second goal was to find the optimal prosthesis stiffness that maximizes the running performance. Moreover, it was wished that the musculoskeletal model resembled a realistic running motion.** Due to some limitations of the study, the aim was scaled down to steady-state running instead of 100 metres sprint.

Four different **research questions** were aimed to be answered:

- Is it an asymmetric running pattern optimal for UTT amputees?
- What is the effect of prosthesis stiffness on running economy and performance?
- What is the effect of prosthesis stiffness on the motion and the running cycle?
- What is the effect of prosthesis stiffness on power generation during the cycle?

In order to achieve these goals, the following **objectives** for this project were formulated:

1. Making a realistic musculoskeletal model of a UTT amputee athlete.
2. Making predictive forward dynamic simulations and optimization of the running pattern with SCONE software.
3. Addressing the mechanical power balance of the optimized motion.
4. Observing the effect of prosthesis stiffness on the motion and power.
5. Validating the simulated motion with experimental data from the literature.

This work is divided into five chapters. Chapter 1 provides a research background with an introduction of the biomechanics of running for UTT amputees and an overview of the RSP. In Chapter 2, the materials and methods employed throughout the project are explained. In this part, a description of the optimization framework used for performing the predicting simulation is explained, together with the musculoskeletal models used, and a detailed explanation of the simulations that were carried out. In Chapter 3, the results of the simulations are presented. In the first part, the amputee subject is compared with an able-bodied subject. In the second part, the effect of the RSP on biomechanics is explained and eventually, a comparison with real data provided from the literature is shown. In Chapter 4, the discussion of the results answering the research questions is posted. Lately, in Chapter 5, conclusions on the research work and future prospects are discussed.

1

Theoretical Background

This chapter introduces the background which constitutes the basis of the project. Section 1.2 summarizes the basic biomechanics of running with a Running-Specific-Prosthesis (RSP), necessary to understand the outcomes of the project. Section 1.1 gives an inside of the RSP's mechanical properties.

1.1. Biomechanics of unilateral transtibial amputees

The motion of a human leg during running consists of a cycle of two alternating phases: the contact or stance phase, and the swing phase. In the contact phase, the foot is in contact with the ground and it is when the force to propel the body forward is generated by the athlete. The swing phase starts and ends with a flight phase when both feet are in the air. An athlete archives the running speed as a consequence of consecutive alteration of stances and flight phases in each running stride. As Figure 1.1 shows, one stride is described as the event between the two consecutive touchdowns of the same foot, which includes two stance phases and two flight phases. Here below, different **spatiotemporal variables** that are usually measured to describe the kinematic of an athlete are presented [31]:

- Stride time: the duration of the event between the two consecutive touchdowns of the ipsilateral foot.
- Step time: the time between two consecutive touchdowns of the contralateral feet. Step time = stride time /2 in symmetric running
- Contact/Stance time: the time the foot is in contact with the ground. It is determined by the time that the ground reaction force (GRF) exceeds 0N in a force plate.
- Flight time: the time between the end of the contact time of one food and the beginning of the contact moment of the contralateral foot.
- Swing time: the time that a foot is not touching the ground. It is calculated by the difference between the total stride time and the contact time.

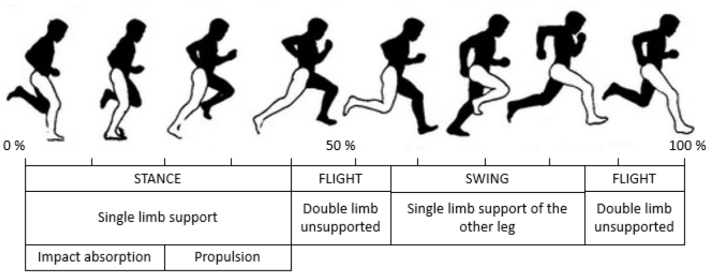

Figure 1.1: Running gait phases by percentage of one stride [18]

Spring-mass model of running

On the other hand, the research community has been interested in examining running biomechanics to understand better how the different parameters affect performance. For that purpose, the mechanics of running is characterized by a spring-mass model where the leg acts as a linear spring (see, Figure 1.2). This behaviour resembles the stretch and recoil of the leg due to the flexion and extension of the hip and knee during the contact phase. During the first half of the stance phase, the spring stores elastic energy which is released along the second half of the stance phase. This allows propelling the body for acceleration in the forward direction. This linear spring is defined by its elastic property, the leg's stiffness (K_{leg}) [2, 27].

In a unilateral amputee, the spring-mass mechanic differs between legs. While the intact leg behaves like one linear spring, the prosthetic leg can be modelled as two in-series springs, the residual limb spring and the RSP spring (see, Figure1.2). In this case, the total prosthetic leg stiffness is highly influenced by the RSP stiffness.

It has been shown that the leg's stiffness is highly correlated with the total power exerted by the leg and therefore, maximal-running-speed. A stiffer spring stretch and recoil quickly and more effectively under large forces, thereby, the transfer of energy is quicker. However, an advantage of a softer spring is that more energy can be stored with the same force. Runners can regulate K_{leg}, by stiffening the muscles, to change the angle swept (θ) and reduce the vertical excursion ($\triangle$y) of the CoM (centre of mass). Leg stiffness might be readjusted by a change in the centrally controlled muscle preactivation [14]. However, in the prosthetic leg, the RSP has a fixed stiffness, which is a clear disadvantage.

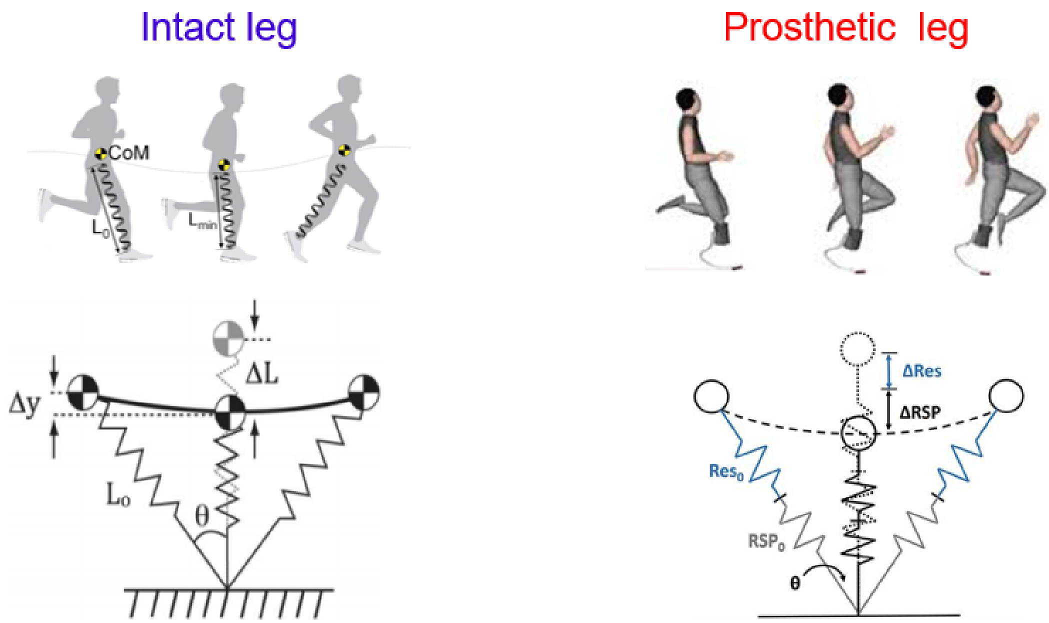

Figure 1.2: Spring-mass models that represent the intact and prosthetic leg mechanics of running. In the intact leg, the spring connects the CoM of the athlete with the foot in contact with the floor. Where $\triangle$y is the vertical excursion, θ the swept angle, L_0 the initial leg length and $\triangle$L the shortened leg during the stance phase of running [2]. The prosthetic leg is modelled as two linear springs, the residual leg spring (Res_0) and the prosthesis spring (RSP_0). The vertical excursion of the prosthetic leg is the sum of the vertical displacement of the residual limb (ΔRes) and the vertical displacement of the prosthesis (ΔRSP).

Leg power

Moreover, unlike muscles, which are able to generate mechanical energy from chemical reactions, the RSP has a passive nature, it stores energy and released it. Therefore, due to missing the ankle joint in the prosthetic leg and the passive nature of the prosthesis, the power generated between legs in a unilateral athlete is expected to be asymmetric. As it is shown in Figure 1.3, the total intact leg power is the sum of the powers exerted by the muscles around the hip, knee and ankle joints. Differently, the total power generated by the prosthetic leg is the sum of the muscle power generated at the hip and knee joints and the power released by the RSP. Therefore, it is expected that the prosthetic's design and mechanical properties play an important role in running performance for the amputee group.

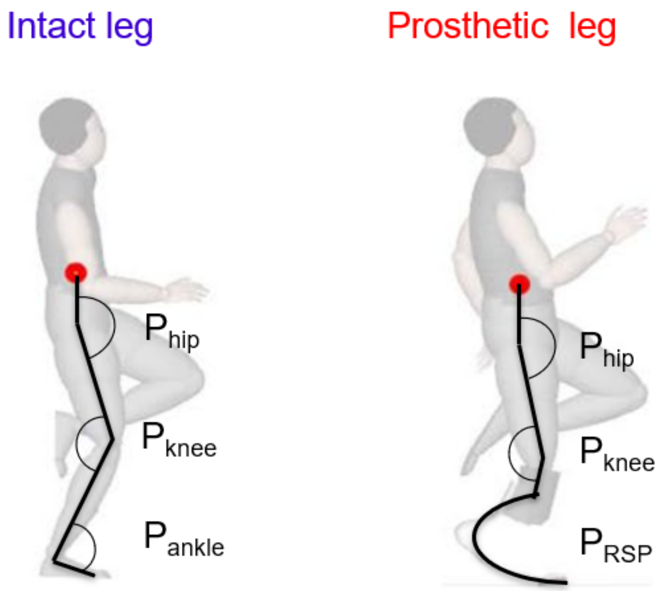

Figure 1.3: Power sources of the intact and prosthetic legs. Total power of the intact leg is the sum of the power at the hip (P_{hip}), at the knee (P_{knee}) and the ankle (P_{ankle}) joints. Total power of the prosthetic leg id the sum of P_{hip}, P_{knee} and power of the prosthesis (P_{RSP}).

1.2. Running-Specific-Prosthesis

In this section, an overview of the current RSP and its mechanical properties will be discussed.

The main purpose of a RSP is to emulate running experience with a biological limb. The principal components of a RSP prescribed for a transtibial amputee are a socket, a blade and the attachment point between both. Firstly, the socket is necessary to fit the prosthesis into the residual leg. It is in direct contact with the skin and has to fit perfectly the form of the leg to maximize the prosthesis' function. Secondly, the blade is manufactured from carbon fibre and is effectively a spring of a passive nature. This spring stores energy when compressing at the touch-down and releases it at the takes-off during running [12].

The energy stored in the RSP is related to its mechanical properties. Adaptations in the blade mechanical properties can be achieved via modifications of the shape design, lamination layout and orientation of the fibres. It seems that the performance of an amputee athlete wearing a RSP can be improved by the adjustment of the **stiffness** distribution of the blade. Currently, manufactures provide blades in different stiffness categories prescribed based on the bodyweight of the athlete (see, Table 1.1). However, for some athletes, a softer prosthesis feels better, and for others a stiffer one, therefore, there is not a straightforward method to recommend a prosthesis to a specific person.

Stiffness category	**Cat 2**	**Cat 3**	**Cat 4**	**Cat 5**	**Cat 6**	**Cat 7**	**Cat 8**
Body weight (kg)	45-52	53-59	60-68	69-77	78-88	89-100	101-116

Table 1.1: Stiffness categories and the subject weight scale for which each RSP is advised [10]

The RSP stiffness (k_{RSP}) can be calculated by the equation of the linear spring (equation 1.1). As it is represented in Figure 1.4, F is the maximal force applied to the ground and $\triangle L$ the deformation of the prosthesis from touchdown to mid-stance. As it can be seen in 1.5.a, the force-displacement curve of a RSP has a curvilinear profile, which indicates that the prosthesis stiffness changes with the magnitude of the force applied.

$$k_{RSP} = \frac{F}{\Delta L} \tag{1.1}$$

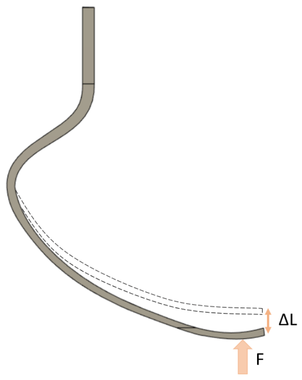

Figure 1.4: Deformation (△L) of a RSP due to a ground contact force (F).

At the same time, the prosthesis stiffness is directly related to the **potential energy stored** in the prosthesis. The energy required to compress or decompress a carbon fibre blade is calculated by integrating the force-displacement curve. In contrast with the structure of the biological leg, which has a damping behaviour, the linear spring of the prosthetic leg is almost completely elastic [7][6]. However, due to friction between the socket and the skin as well as the blade and the ground surface, the spring is not 100% efficient and there is energy lost. This loss is the difference between the potential elastic energy stored and the energy returned and it is called **hysteresis** (see, Figure 1.5.b). The hysteresis is related to the efficiency (η) of the RSP, which can be calculated as (1.2):

$$\eta = \frac{E_{returned}}{E_{stored}} 100\% \tag{1.2}$$

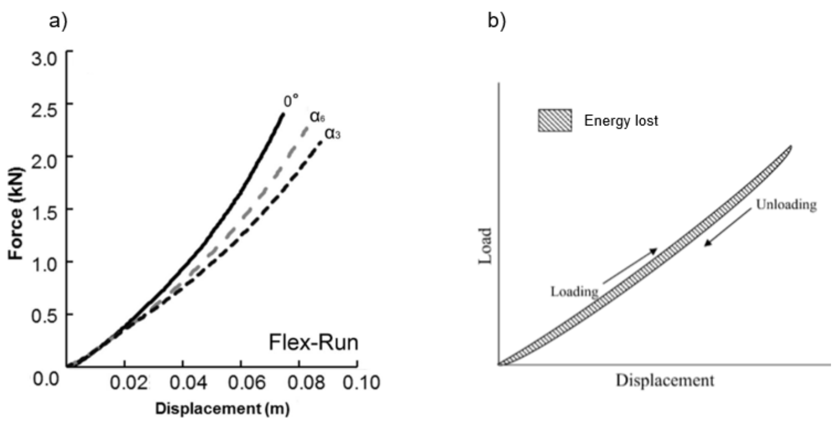

Figure 1.5: a) Force-displacement curve of a Flex-Run (Ossur) RSP. α angles regard the measured angles between the RSP and the resultant ground reaction force (GRF) vector[6]. By integrating this curve, potential elastic energy is obtained. b)Loading/Unloading displacement curves. Grey section represents the hysteresis of the prosthesis [19].

Moreover, in Figure 1.5.a is shown that the **alignment** on the sagittal plane of the prosthesis also influence k_{RSP}. Increasing the angle of the RSP with respect to the resultant GRF vector decreases the k_{RSP} [6]. Besides, the sagittal plane angle of the RSP also defines the position of the athlete CoM concerning the contact point (CP) of the prosthesis with the ground. When the contact point of the prosthesis is posterior to the CoM, the GRF vector connected with the CoM is positive in the horizontal direction, therefore forward acceleration is developed. However, when the force is applied anterior to the CoM, the GRF vector is negative in the horizontal direction and forward acceleration is restricted (see, Figure1.6).

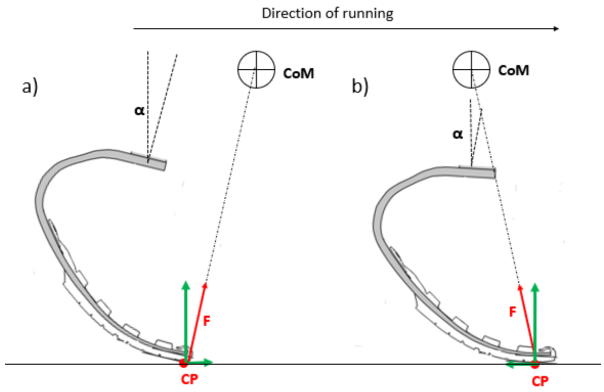

Figure 1.6: Influence of the alignment angle α on the GRF vector direction. a) If the CoM is posterior to the contact point (CP), a positive horizontal force is produced. b) If CoM is anterior to the CP, a horizontal force in the negative direction is generated, limiting forward acceleration.

2

Materials and Methods

The reproduction and analysis of the running gait of an amputee subject running with a Running-Specific-Prosthesis were approached by predictive forward dynamic simulations using Scone software [9]. Predictive forward dynamic simulations use a controller that regulates the motor inputs of a musculoskeletal model and the emerged trajectory is analysed and optimized based on an objective function. The Scone platform facilitates a sensory feedback control algorithm, based on Neural Networks, for running gait and the optimization algorithm of the controller parameters. To solve the optimization problem, Scones uses Covariance Matrix Adaptation Evolutionary Strategy (CMA-ES). Figure 2.1 shows a scheme of the optimization framework.

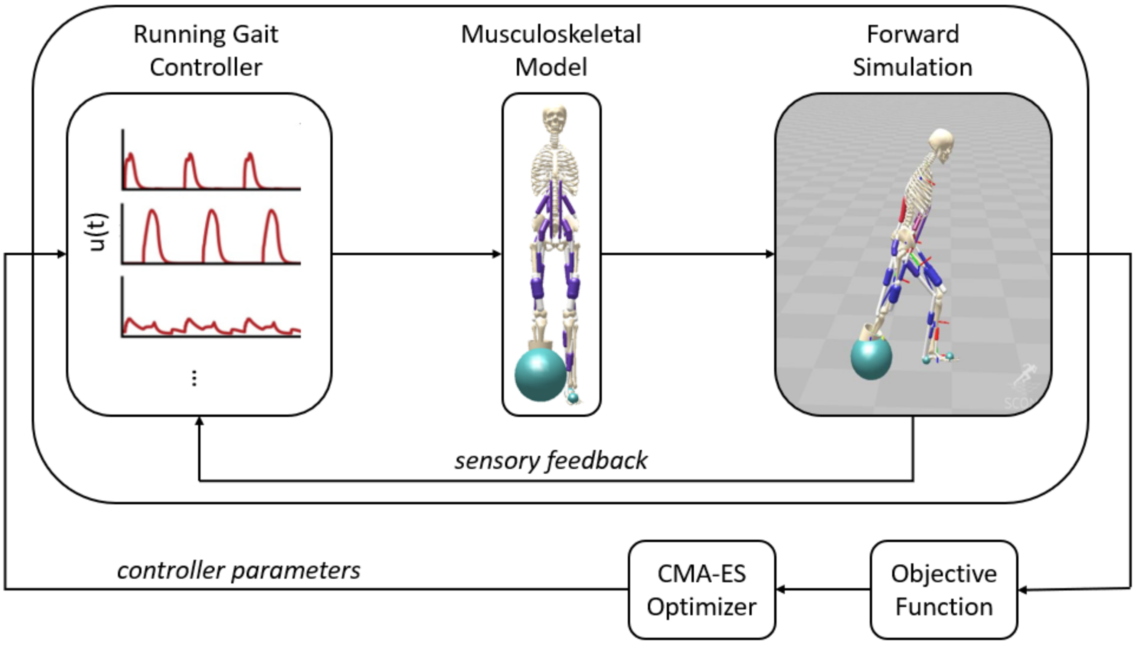

Figure 2.1: Framework used for the dynamic optimization. Two planar musculoskeletal models, one healthy athlete and one amputee athlete, were trained to run by optimizing the parameters of a running gait controller with an objective function. The objective function aimed to minimize the metabolic cost, avoid falling, knees hyperflexion and leaning forward. The running gait controller estimated the muscles excitations, u(t), that were the input of the musculoskeletal model to perform a forward simulation. The muscles model's sensory parameters (length, velocity and forces) of the emerged motion were introduced in a feedback loop with the running gait controller. On the other hand, the performance of each simulation was assessed by the objective function and in each iteration, the values of the parameters in the optimization problem were updated by Covariance Matrix Adaptation Evolutionary Strategy (CMA-ES). The present optimization framework was based on the previous study made by Carmichael F. Ong et al[21].

Following in this chapter the materials and methods used in this project are presented. First, the musculoskeletal models are described. Second, the optimization and simulation framework is explained, with a detailed description of the objective function and the simulations settings. Third, a characterization of the mechanical power of the emerged motion is raised.

2.1. Musculoskeletal model

Two musculoskeletal models were used in this study, one healthy subject, which was based on a previous full-body, no arms OpenSim model, Delp et al, 1990 [8], and one amputee subject, which was an adaptation of the healthy one. The healthy individual was about 1.8 m tall and weighed 83.5 kg, while the amputee weighted 81.43 kg without prosthesis and had a prosthesis mass with the socket included of 1.3 kg. Both models were developed on Hyfydy extension. Here bellow the unilateral transtibial amputee musculoskeletal model is detailed explained as the healthy subject was the symmetrical version of the amputee.

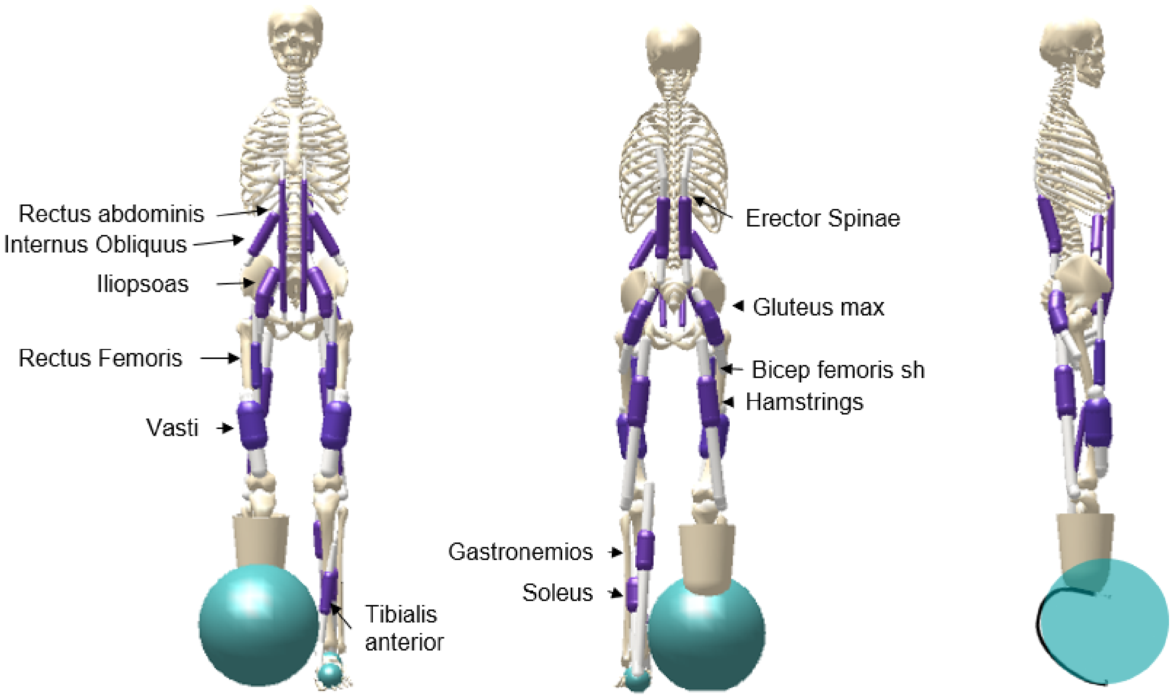

Figure 2.2: Unilateral transtibial amputee musculoskeletal model. It consisted of 8 segments, 10 degrees of freedom (dof) and 21 Hill-type muscle-tendon-units. Three dof planar joint that linked the ground and pelvis. Four 1 dof joints of each hip and knee, 1dof of the intact leg ankle, 1 dof for the socket joint and 1dof for the lumbar extension. The main group muscles were: gluteus maximus, hamstrings, biceps femoris short head, iliopsoas, rectus femoris, vasti, gastrocnemius, soleus and tibialis anterior. Moreover, a Flex-Run^{TM} RSP (Ossur, Reykjavík, Iceland) was modelled as a compliant Hunt-Crossley contact model, with a contact sphere placed in the socket.

As it is shown in Figure 2.2, it was a planar model with 8 segments and 10 degrees of freedom (dof). Three dof planar joint that linked the ground and pelvis. Four 1 dof joints of each hip and knee, 1dof of the intact leg ankle, 1 dof for the socket joint and 1dof for the lumbar extension. Mass and inertia properties of each body are summarized in 2.1.

First, in order to adjust the model from the healthy subject, 40% of the right tibia was cut and the right foot was removed. Mass and inertia of the residual tibia were adjusted to the 60% of the healthy tibia. Second, the amputated tibia and foot were substituted by a type Flex-Run^{TM} RSP (Ossur, Reykjavík, Iceland) with a socket adjusted to the tibia. Mass, inertia tensor and centre of mass of the prosthesis, with the socket included, were taken from Baum et al. [4] study. Besides, the socket geometry was provided by LaPre et al [17].Lastly, the right ankle dof was replaced by the socket connection to the residual leg. The impedance that occurred at this joint was modelled as a nonlinear torsional spring, which produced a high torque for the whole dof range of movement, plus a stiff transnational spring-damper (stiffness constant of 1.000.000 N/m). It resembled almost a weld joint.

Segment	mass (kg)	Ixx	Iyy	Izz
Torso	35.40	1.5246	0.7811	1.4800
Pelvis	13.09	0.1143	0.0968	0.0640
Femur	11.93	0.1717	0.0450	0.1811
Tibia	4.31	0.0586	0.0059	0.0595
Calcaneus	1.25	0.0014	0.0039	0.0041
Tibia amputated	2.22	0.0302	0.0030	0.0307
Prosthesis	1.30	0.0317	0.0030	0.0370

Table 2.1: Segments mass and inertial properties used.

Furthermore, the model was actuated using 21 Hill-type muscle-tendon units. Nine for the intact leg, six for the prosthetic leg and six for the torso. Leg muscles that have similar functionality in the sagittal plane were grouped into a single muscle with summed peak isometric forces. The main muscles groups were: gluteus maximus, hamstrings, biceps femoris short head, iliopsoas, rectus femoris, vasti, gastrocnemius, soleus and tibialis anterior. The prosthetic lacked of the three muscles located at the shank, gastrocnemius, soleus and tibialis anterior. The torso was actuated with two rectus abdominis, two internal obliques and two erector spinaes. Tendon-slack lengths, optimal muscle lengths and pennation angles remained the same as the Delp et al, 1990 [8] model.

Muscle force scaling

On the other hand, maximum isometric muscle forces were scaled accordingly to a healthy sprinter total lower limb muscle volume (V_{total}), which was 11095 cm^3 [20]. First, the individual muscle volumes were calculated based on the mean lower limb muscle volume fraction (ϕ^{m}) of each muscle, reported in the Handsfield et al study [13]. Second, the muscle physiological cross-section area (PCSA) was determined as each muscle volume divided by its optimal fiber length (${l^{\text{m}}}_0$). Assuming that the maximum isometric fiber force (${F^{\text{m}}}_0$) is directly proportional to the PCSA, it can be estimated as 2.1:

$$F_0^m = \sigma_0^m \frac{\phi^m V_{total}}{l_0^m} \tag{2.1}$$

where ${\sigma^{\text{m}}}_0$ is the specific tension. A ${\sigma^{\text{m}}}_0$ of 60N$/cm^2$ was chosen, as it is in the range of mammalian muscles, and it was previously used in others musculoskeletal models [24]. In Table 2.2 the muscle-tendon parameters are collected.

Third, in order to scale the model realistically, the additional muscle mass was added to the segment's mass of the reference model. In addition, the segments inertia properties were also scaled by the same rate as the segment mass. Table 2.1 shows the mass and inertia properties of each body.

Muscle	${F^{\mathbf{m}}}_{\mathbf{0}}$ (N)	$\phi^{\mathbf{m}}$	${l^{\mathbf{m}}}_{\mathbf{0}}$ (m)	${l^{\mathbf{m}}}_{\mathbf{t}}$ (m)	Pennation angle
Glut max	5434	0.12	0.147	0.127	0
Iliopsoas	4660	0.07	0.1	0.163	0.139
Rectus Femoris	2277	0.039	0.114	0.31	0.087
Vasti	13563	0.218	0.107	0.116	0.052
Hamstrings	7023	0.115	0.109	0.313	0
Bicep Femoris short head	654	0.017	0.173	0.071	0.401
Soleus	7188	0.06	0.05	0.25	0.436
Grastronemios	6129	0.058	0.063	0.39	0.297
Tibialis anterior	2717	0.04	0.098	0.223	0.087
Rectus abdominis	800	0.04	0.333	0.082	0
Erector Spinae	3305	0.07	0.141	0.2	0
Internus Obliquus	2663	0.04	0.1	0.1	0

Table 2.2: Muscle-tendon parameters of the individual muscles and their lower limb muscle volume fraction ϕ^{m}. ${F^{\text{m}}}_0$ is the maximum isometric force , ${l^{\text{m}}}_0$ the optimal muscle length and ${l^{\text{m}}}_{\text{t}}$ the tendon slack length

In addition, ligaments were modelled as nonlinear rotational springs-damper at the joints. Ligaments produced torque when the joints exceeded beyond their natural limits, to avoid their hyperextension or hyperflexion. Hip and ankle joints generated torque when they were flexed or extended above 180º. Knee joints were limited when flexed beyond 90°and extended beyond 0º. Lumbar extension joint generated a soft torque beyond 0º extended and flexed.

On the other hand, the soft tissue at the joint's cavities, such as the cartilage, and the impedance of the socket c was modelled as quite stiff linear spring-damper between the segments. The stiffness constant was equal for all the joints, 1.000.000 N/m while damping was set automatically to critical damping by SCONE.

Moreover, a compliant Hunt-Crossley contact model [23] was used in order to create the force produced due to the contact between the intact leg foot with the ground. The foot had two contact spheres, one at the toes and another one at the heel. Both spheres had a radius of 3 cm, plane strain modulus of 2,700,000 N/m, a static and dynamic friction coefficient of 0.9 and a dissipation coefficient of 1 s/m.

Running-Specific-Prosthesis model

Finally, the spring behaviour of the RSP carbon-fibre blade was modelled as a compliant Hunt-Crossley contact model, with a contact sphere placed in the socket. This is an original approach to model a RSP. Several studies [16, 25] resembled the shape and stiffness of the blade as multi-linked segments joined by torsional springs. However, this was avoided as the small mass of the segments could cause vibrations in the simulations. A contact sphere with a Hunt-Crossley stiffness and dissipation model allowed to represent the RSP blade with no mass and therefore prevents oscillations. The total mass of the RSP and its inertia properties were implemented together with the socket body. Moreover, the non-linear deformation behaviour of the HuntCrossley model could resemble properly the stiffness dependency on the applied force of a RSP [6].

The sphere was located in the way that the prosthetic leg was 3 cm longer than the intact leg, as it was set in Beck et al [5] study. The angle of alignment on the sagittal plane was installed to a 9º flexion angle, as it is in the range that is normally prescribed. Moreover, the centre of the sphere was located in the way that the contact surface of the sphere with the ground had the same curvature as the real prosthesis. The location of the centre of the sphere with respect to the RSP CoM is shown in Figure 2.3. The static and dynamic friction coefficient was established to 0.9 and the dissipation coefficient to 0.2 s/m. On the other hand, the plane-strain modulus was calculated using real data of the force-displacement of a blade and applying the equation 2.2, of the Hertz stiffness model with Hunt and Crossley dissipation model. However, we assumed that there was no dissipation (c) to avoid solving an undetermined differential equation. Therefore, the Hunt and Crossley force (f_{HC}) was equal to the Hertz force (f_{H}) (eq. 2.3), where Δy is the penetration depth of the sphere, R its radius and E is the plane-strain modulus.

A test was performed to measure the blade displacement in the y-axis (Δy) for a specific applied force in static conditions. The blade taken to perform the test was recommended for an athlete of about 40 kg. This corresponds to a stiffness category 2, which was really soft for our athlete. However, it served as a reference to estimate the displacement it would occur in a category 6 that matched our athlete bodyweight requirements. Beck et al [6] and Oudenhoven et al[22] studies were used as an example to calculate the prescribed stiffness.

$$f_{HC} = f_H(1 + \frac{3}{2}cv) \tag{2.2}$$

$$f_H = \frac{4}{3}\sqrt{R}E(\Delta y)^{3/2} \tag{2.3}$$

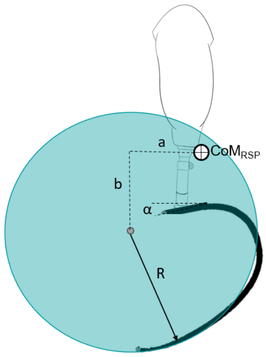

Figure 2.3: Location of the centre of the RSP contact sphere with respect to the CoM of the RSP (CoM_{RSP}), a was equal to 0.069 m, b to 0.0693 m and R = 0.1464 m. α is the angle alignment on the sagittal plane, which was set to 9°. CoM_{RSP} was estimated by Baum et al [4].

As we were interested in observing the effect of the RSP stiffness on motion, five different stiffness categories were tried in our athlete. Table 2.3 collects the RSP categories used, their corresponding stiffness, plane-strain modulus of the contact model and the stiffness divided by bodyweight of the athlete.

Stiffness category	BW (kg)	Stiffness RSP (kN/m)	E (N/m)	kN/kg/m
Cat4	60-68	21.2	625.890	0.294
Cat5	69-77	24.23	705.740	0.336
Cat6	78-83	27.3	804.130	0.377
Cat6 High	83-94.5	30.3	927.720	0.42
Cat7	94.5-100	33.3	1.086.600	0.466

Table 2.3: Stiffness categories used in our simulations recommended per body weight, of a Flex-RunTM RSP (Ossur, Reykjavík, Iceland), to run at 4 m/s [6]. Cat6 was the one prescribed for a 80 kg a person. Stiffness RSP and E regard the corresponding stiffness and plane-strain modulus for each stiffness category. On the other hand, kN/kg/m concerns the stiffness per body weight of our athlete.

2.2. Simulation and optimization framework

In this section, the objective function used for all the simulations as well as the different simulations scenarios carried out to achieve the results of this thesis are described.

2.2.1. Objective function

In order to assess the parameters defined, an objective function J (see, equation2.4) was established. It quantified the running performance and it was desired to minimize it.

$$J = w_{cot}J_{cot} + w_{gait}J_{gait} + w_{inj}J_{inj} + w_{leaning}J_{leaning} \tag{2.4}$$

The function J, aimed to minimize the metabolic cost (J_{cot}), while avoiding falling during running at constant prescribed speed (J_{gait}), knee ligaments injuries (J_{inj}), and leaning backwards (J_{leaning}). The weights were decided to priorities finding solutions that penalize the different objectives as follow: w_{cot} = 0.1 kg·m/J, w_{gait} = 100 s-1, w_{inj} = 0.1 N^{-1}, and w_{leaning} = 0.1 $degrees^{-1}$. Our objective function prioritized finding solutions that avoid failing before minimizing cost of transport, and lastly avoiding ligament injuries and leaning backwards. All these functions were already implemented in Scone. Here below, a description of every function is presented.

Simulations in which the athlete run less metabolically efficient were penalized by J_{cot}. J_{cot} was calculated as the gross metabolic rate ($\dot{E}$) over the simulation time and divided by the bodyweight of the model (m) and the distance travelled (d) (see, equation 2.5). The gross metabolic rate was the sum of the basal metabolic cost and the sum of each muscle metabolic rates. In order to calculate $\dot{E}$, the metabolic model described in Uchida et al [29] was used.

$$J_{cot} = \frac{\int_0^{t_{end}} \dot{E} dt}{md} \tag{2.5}$$

Moreover, J_{gait} punished simulations in which the model fell before the desired simulation end time (t_{des}) or had a step velocity not within the prescribed speed range [v_{min}, v_{max}].

$$J_{gait} = 1s - \sum_s \frac{t_s v_{s,pen}}{v_{min}} \tag{2.6}$$

$$v_{s,pen} = \begin{cases} 0, & t_{end} = t_{fall} \\ max[0, 1m/s - \Psi(v_s, v_{min}, v_{max})], & t_{end} = t_{des} \end{cases} \tag{2.7}$$

$$\Psi(\varphi, \varphi_{min}, \varphi_{max}) = \begin{cases} 0, & \varphi_{min} < \varphi < \varphi_{max} \\ \varphi_{min} - \varphi, & \varphi < \varphi_{min} \\ \varphi - \varphi_{max}, & \varphi > \varphi_{max} \end{cases} \tag{2.8}$$

where s refers to a step, t_s denotes the duration of a step, $v_{s,pen}$ concerns the penalty for a step and ranges between 0 and 1, being 1 no penalty, v_s is the velocity of a given step, t_{fall} defines the moment at which the model fall, and Ψ determines a linear penalty if v_s is not between v_{min} and v_{max}.

Lastly, J_{inj} penalized simulations where the knee dof experienced load outside the range -100N to 100N. Likewise, $J_{leaning}$ penalized simulation when the pelvis tilt dof was not within the range -16º to -2º. These penalties were computed as it is described in equation 2.9, where Err is the amount a value is out of range and *penalty* was equal to 1.

$$Penalty = abs(penalty)|Err| + penalty^2 Err \tag{2.9}$$

2.2.2. Simulations scenarios

In order to perform the simulations a duration time of 10 seconds was desired, and an integrator accuracy of 0.01 was used.
There are four elements to consider for making the forward dynamic simulations: the initial values of the parameters to be optimized, the initial state values, the model and the measures that define the objective function. All the simulations used the same initial state values, which were taken from previous simulations on the healthy subject. Moreover, the initial values of the parameters were also taken from previous simulations of a healthy subject. Here bellow, the approach followed to perform the simulations included in this report are detailed described.

A) Starting point simulations
First, the healthy subject and the amputee subject, wearing a Cat6 stiffness category RSP model, were trained with free parameters optimization. Twenty parallel optimizations with a self-selected minimum speed of 3 m/s were performed, until some of them reached a solution. It was observed that models with higher inertia properties and muscle force were more difficult to be optimized, therefore, one scaled-down model was taken for the first optimization. Second, this solution was used as initial values of our desired solution models. Third, a higher prescribed speed, 3.5 m/s was optimized for the final comparison of the motion between healthy and amputee subject.

B) Generating simulations for different stiffness categories.
Once we had the desired motion for the amputee subject running at 3.5 m/s, simulations for the different prosthesis stiffness mentioned in Table 2.3 were carried out at the same prescribed speed. Cat6 served as the initial values of Cat5 and Cat6High. After, solutions from Cat5 and Cat6High were used to optimize Cat4 and Cat7 prosthesis respectively. For each simulation, 6 parallel optimizations were executed.

C) Generating simulations for reaching maximum speed.

To compare the performance of the amputee athletes wearing different prostheses, we performed simulations for increasing self-selected velocities. The velocity was raised 3 times, to 4 m/s, 4.5 m/s and 5 m/s. The solutions of each prosthesis model from previous velocities were used as an initial value of the same prosthesis for the next velocity. All models achieved 4 m/s, however, some of them did not reach 4.5 m/s and non of them 5 m/s. The ones that reached more than 4.5 m/s were two times optimized with a prescribed speed of 5m/s till the solution did not change.

D. Generating simulations for validation of the model

Firstly, two new simulations of the amputee subject wearing Cat6 and the healthy subject running at 3.5 m/s were performed in order to compare the motion with Sepp et al [26] study. The subjects weights were matched to the mean of the participants of the article and their muscle masses and inertial properties were also reduced 20%, as they were not professional athletes.

Secondly, the original amputee athlete model was used to contrast the data with Beck et al [5] study. For that purpose, the RSP stiffness used by the athlete had to be figured out, as he used a Cheetah Xtreme (Ossur, Reykjavik, Iceland) model. This was approached by matching the contact time of the prosthetic leg of the simulation as close as possible to the experimental data for one velocity. It turned out that he used a quite soft prosthesis for his body weight, a Cat5 stiffness category. Then, the velocity was increased by 0.1 m/s till reaching the maximum velocity of the model.

2.3. Analysis of the Mechanical Power

After performing the simulations, the power balance of our healthy and amputee models was computed for verification.

Mechanical power can be an indication of performance in endurance sport, as gives an insight into the capability of the athlete to produce power. For this reason, it is often used by scientists, athletes and coaches for training aims. It can be calculated by applying the classic biomechanics laws, modelling the body as a linked segment [30].

Muscle power results in mechanical power, without considering non-conservative power, due to heat and friction inside the body, and power against conservative forces like tendon stretch, which can be used again. Therefore, it is possible to estimate muscle power by the calculation of mechanical power in a musculoskeletal model. For this reason, power balance equations serve also as a tool to verify that the mechanics behind the musculoskeletal model is correct.

The mechanical power balance equations of our musculoskeletal model consisted of four terms: muscle power ($\mathrm{P_m}$), produced by the human, joint ligaments power ($\mathrm{P_{lj}}$), produced by the ligaments and soft tissue inside the joints, contact power ($\mathrm{P_c}$), caused by the deformation of the prosthesis and the shoe in the intact leg when hitting the ground, gravitational power of the body ($\mathrm{P_g}$), and emerged kinetic power in the segments ($\mathrm{P_k}$). To meet the power balance in our model the following equation must be fulfilled.

$$P_{external} = P_k \tag{2.10}$$

$$P_m + P_{jl} + P_c + Pg = P_k \tag{2.11}$$

Muscle power

$\mathrm{P_m}$ was the sum of the individual muscles power. The power produced by each muscle,i, was computed as the multiplication of its tendon force, $\mathrm{F_t}$ and the contraction velocity of its muscle-tendon unit, v_{mtu}.

$$P_m(t) = \sum_{i=1}^{\#muscles} F_{t,i}(t)\, v_{mtu,i}(t) \tag{2.12}$$

Joint ligament power

The power produced inside the joint, j, was divided into transitional ($\mathrm{P_{tr}}$) power and rotational power ($\mathrm{P_{ro}}$). The translational element regards the cartilage between the joints, which was modelled as a linear-spring damper system, and the rotational part of the ligaments at the joints modelled as torsional linear spring-damper.

$$P_{jl}(t) = P_{tr,j}(t) + P_{ro,j}(t) = F_{tr,j}(t)v_{tr,j}(t) + \theta_j(t)\dot{\theta}_j(t)k \tag{2.13}$$

Where F_{tr} regards the translational force produced at the joints, v_{tr} the translational velocity of the displacement inside the joint, θ the joint angle, $\dot{\theta}$ the joint angular velocity and k the rotational stiffness of the joint limit.

Ground contact power
The contact force between the healthy foot and the prosthesis with the ground produced power due to the deformation of the contact models. As it was mention in Section 2.1, Hunt-Cross (HC) Ley contact model was chosen to represent the contact between the prosthesis and the shoe with the ground. Equation 2.14 describes the potential energy stored in a HC Ley model ($E_{p,HC}$) due to the deformation of the sphere (Δy) when hitting the ground with a ground-reaction-force F_{grf}. In addition, equation 2.3, shown in Section 2.1, was used to calculate Δy at every moment in time. Then, potential powers of the prosthesis ($P_{p,HC,RSP}$) and the shoe ($P_{p,HC,shoe}$) were computed as described in equation 2.15. Finally, the P_c was the sum of both contact, the shoe and the prosthesis.

$$E_{p,HC}(t) = \frac{2}{5}F_{grf}(t)\Delta y(t) \tag{2.14}$$

$$P_{p,HC}(t) = \frac{\partial E_{p,HC}(t)}{\partial t} \tag{2.15}$$

$$P_c(t) = P_{p,HC,RSP}(t) + P_{p,HC,shoe}(t) \tag{2.16}$$

Gravitational power
The total gravitational power of the body was calculated with the sum of the individual segments, s, gravitational power.

$$P_g(t) = \sum_{s=1}^{\#segments} v_s(t)m_s g \tag{2.17}$$

Where v_s is the translational velocity of the segment in the y-axis, m_s the mass of the segment and g the gravity.

Segment kinetic power
Lastly, the rate of the total body kinetic energy change was determined as the sum of kinetic powers of the individual segments. The segment kinetic power consists of the sum of the transitional $P_{k,tr}$ and rotational $P_{k,ro}$ terms, as it is describes in equation 2.18.

$$P_k(t) = P_{k,tr,s}(t) + P_{k,ro,s}(t) = \sum_{s=1}^{\#segments} m_s a_s(t)v_s(t) + \sum_{s=1}^{\#segments} I_s\dot{\omega}_s(t)\omega_s(t) \tag{2.18}$$

Where m is the mass, a the linear acceleration, v the linear velocity, I the inertia, $\dot{\omega}$ the angular velocity and ω the angular velocity, of each segment.

2.4. Analysis of the total leg stiffness

As it was mention in Section 1.1, the spring-mass model of running is characterized by its Kleg. Leg stiffness of our simulations was calculated following the approach described in Beck et al [5], where Kleg is the fraction between the peak vertical GRF (F$peak$) and the peak leg spring compression (ΔL).

$$K_{leg} = \frac{F_{peak}}{\Delta L} \tag{2.19}$$

Moreover, ΔL is usually calculated with equation 2.20. Where Δy is the peak vertical displacement of the CoM during the contact time, L0 the initial leg intact and prosthetic leg lengths, and θ the angle swept. θ was computed as shown in equation 2.21, where v regards the running velocity and t_c the contact time.

$$\Delta L = \Delta y + L_0(1 - cos\theta) \tag{2.20}$$

$$\theta = sin^{-1}(\frac{vt_c}{2L_0}) \tag{2.21}$$

3
Results

In this chapter, the results of the simulations are presented. First, the differences in biomechanics of the healthy subject compared with the amputee subject are discussed. Second, the effect of adjusting the RSP stiffness on the amputee's running biomechanics, in order to find the optimal stiffness, is posed. Lastly, the accuracy of the simulations is assessed by comparing them with real data provided in the literature. In the upcoming results, healthy refers to the leg of the able-body subject, intact to the biological leg of the amputee subject and prosthetic to the amputated leg.

3.1. Amputee running biomechanics compares with able-bodies

To get an idea of the amputee running biomechanics, in this section an observation of the motion, spatiotemporal variables, GRFs, power balance, of the amputee subject compared with the healthy subject is presented. Both subjects were imposed to run at 3.5/s. Moreover, a Cat6High stiffness category was chosen for the amputee's RSP. The simulations scenarios carried out to achieve the following results are explained in Section 2.2.2.B.

A. Motion

Figure 3.1 illustrates the differences in motion between the healthy and the amputee runners during one gait cycle, from touch down to touch down. It can be observed that the healthy leg exhibited a higher peak hip extension angle (-10.7º) and lower peak hip flexion angle (44º) than the intact leg (-5º peak hip extension angle and 48.7º peak hip flexion angle). The prosthetic leg showed a greater peak hip extension angle (5.5º) and a smaller peak hip flexion angle (36.4º) than the intact leg. It also appeared that the healthy subject ran more leaning forward than the amputee subject, as the hip angle of the full gait cycle had a negative offset of the intact leg. In addition, the peak knee flexion angle was larger in the intact leg (77.8º), than in the healthy (57.4º) and prosthetic leg (52.3º). Furthermore, regarding the peak ankle angles, the healthy leg used a higher peak plantarflexion angle (-26.3º) at the take-off and a smaller peak dorsiflexion angle (4.8º) during the swing phase than the intact leg ankle (-4.15º plantarflexion angle and 11.6º dorsiflexion angle).

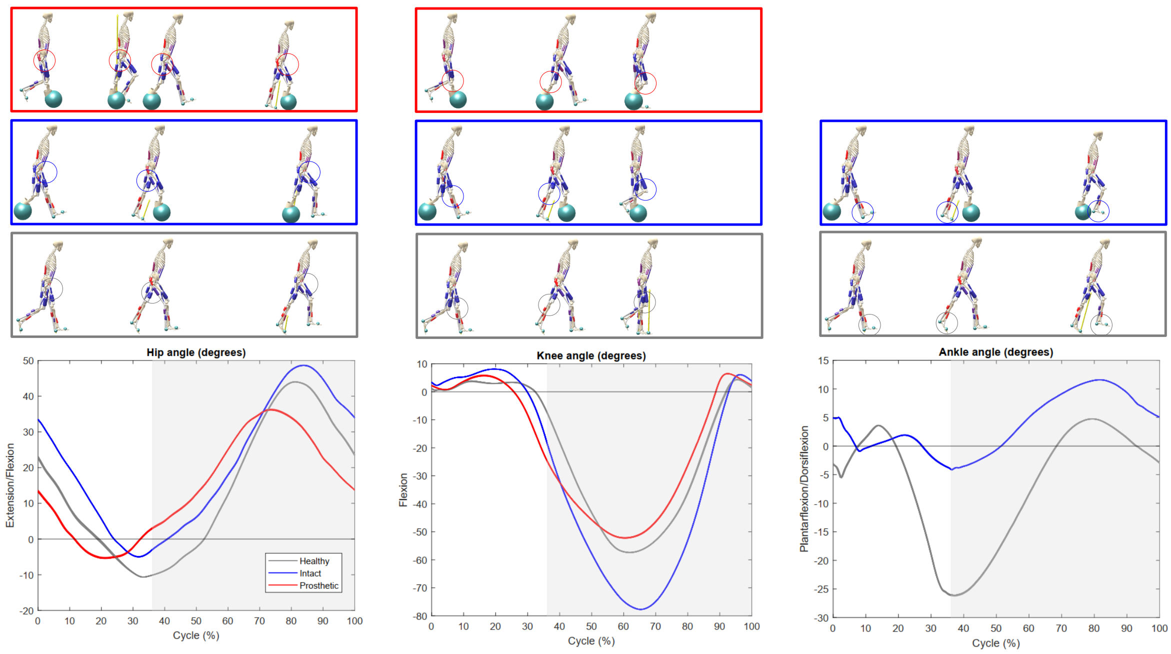

Figure 3.1: Joint angles of the healthy, intact and prosthetic legs normalized by the percentage of the gait cycle for each leg.

B. Spaciotemporal variables

Furthermore, spatiotemporal variables of both subjects are displayed in Figure 3.2. Stride time was longer in the healthy subject (0.55 s) than in the amputee subject (0.48 s). Healthy leg presented greater contact and flight times (0.18s and 0.095s respectively) than both legs of the amputee subject's legs. Moreover, asymmetry in contact and flight times is seen between the legs of the amputee. The intact leg had a contact time of 0.17s while the prosthetic leg of 0.16s. Flight time of the intact leg was 0.09s and of the prosthetic leg was 0.05s.

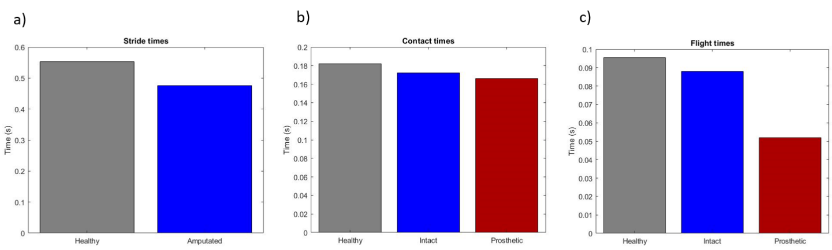

Figure 3.2: a) Stride times of the healthy (grey) and amputated (blue) subjects. b) Contact times and c) flight times of the healthy (grey), intact (blue) and prosthetic (red) legs.

C. Ground reaction force

Figure 3.3 illustrates the GRFs in the horizontal and vertical direction normalized by the body weight and by the percentage of each leg stance phase. Regarding the horizontal GRF, the healthy leg presented a higher peak braking force, being -0.48 BW (times body weight), than the intact leg (-0.20 BW) and the prosthetic leg (-0.35 BW). Peak propulsive forces at the end of the stance phase resulted to be higher in the healthy leg (0.22 BW) than in the intact (0.2 BW). Moreover, the prosthetic leg exerted a quite low peak propulsive force (0.12 BW) compare with the biological legs. On the other hand, concerning the vertical GRF, the healthy leg had the highest peak force (3.85 BW) compared with the amputee subject's limbs. In addition, the prosthetic leg appeared to have a lower peak vertical force (2.7 BW) than the intact leg (2.84 BW).

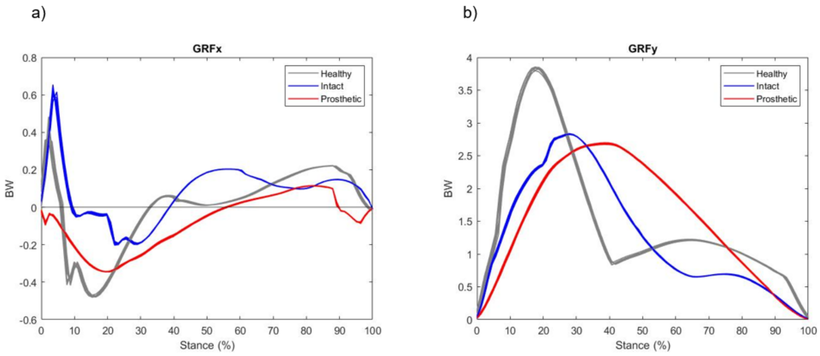

Figure 3.3: Ground reaction force (GRF) on a) x-axis and b) y-axis of the healthy (grey), intact (blue) and prosthetic legs (red) by the percentage of the stance phase.

D. Power

Besides, the power balance approach described in Section 2.3 was applied for both subjects in order to verify the equations of motion. Both subjects met the power balance equation as the total segment power and total external power summed up to zero. In Figure 3.4 the amputee total segment power and total external power are shown to be equal. It can be observed that the amputee subject presented an asymmetry in power generation and dissipation between the intact leg stance phase and the prosthetic leg stance phase. There was less total power generated in the segments and more power dissipated at the stance phase of the prosthetic leg than at the stance phase of the intact leg.

From analysing the individual power sources (see, Figure A.2 in Appendix A), it can be drawn that most power generated came from the muscles as well as the prosthesis spring during the contact of the prosthetic leg. Moreover, most power dissipated in the segments occurred due to the shoe touch-down, in the healthy and intact legs, and due to the prosthesis touch-down in the prosthetic leg.

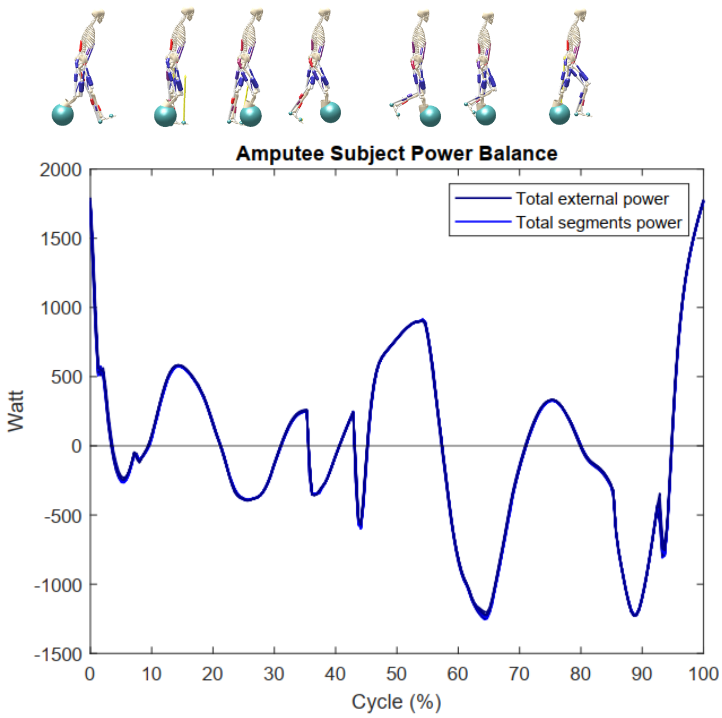

Figure 3.4: Power balance of the amputee subjects by percentage of the gait cycle (from touchdown to touchdown of the intact leg). Total external power = Total segments power.

Further analysis of individual segments power and individual muscles power contribution was carried out. High-frequency oscillations were presented in the segments and muscles powers. Especially on the torso and femur (see, Figure A.3b in Appendix A), and therefore the changes in the muscles length were affected as well. However, this did not have a significant effect on the overall results.

Figure 3.5 shows the total muscles power developed around the hip, knee and ankle joints, in the healthy, intact and prosthetic leg. The prosthetic leg produced reduced muscle power than the intact leg in the amputee subject. Specifically, the prosthetic leg generated 50.4% less hip muscle power and 97.7% lower knee muscle power than the intact. Moreover, 40.4% more power was generated at the hip and 85.2% at knee joints by the intact leg than the healthy leg. Surprisingly, the intact leg ankle power was 79.3% lower than in the healthy leg. In addition, the RSP exerted 7.15 times more power than the intact leg ankle. That is probably because the RSP was very stiff to run at 3.5 m/s and the intact ankle did not need to generate any power.

Furthermore, the main muscles responsible for generating power were the gluteus maximum, iliopsoas, hamstrings, and gastrocnemius. The muscles from the prosthetic leg did not exert as much power as the muscles from the intact leg, especially the gluteus maximum and the hamstrings (see, Figure 3.6). The raw results from the rest of the muscles can be seen in Appendix A.

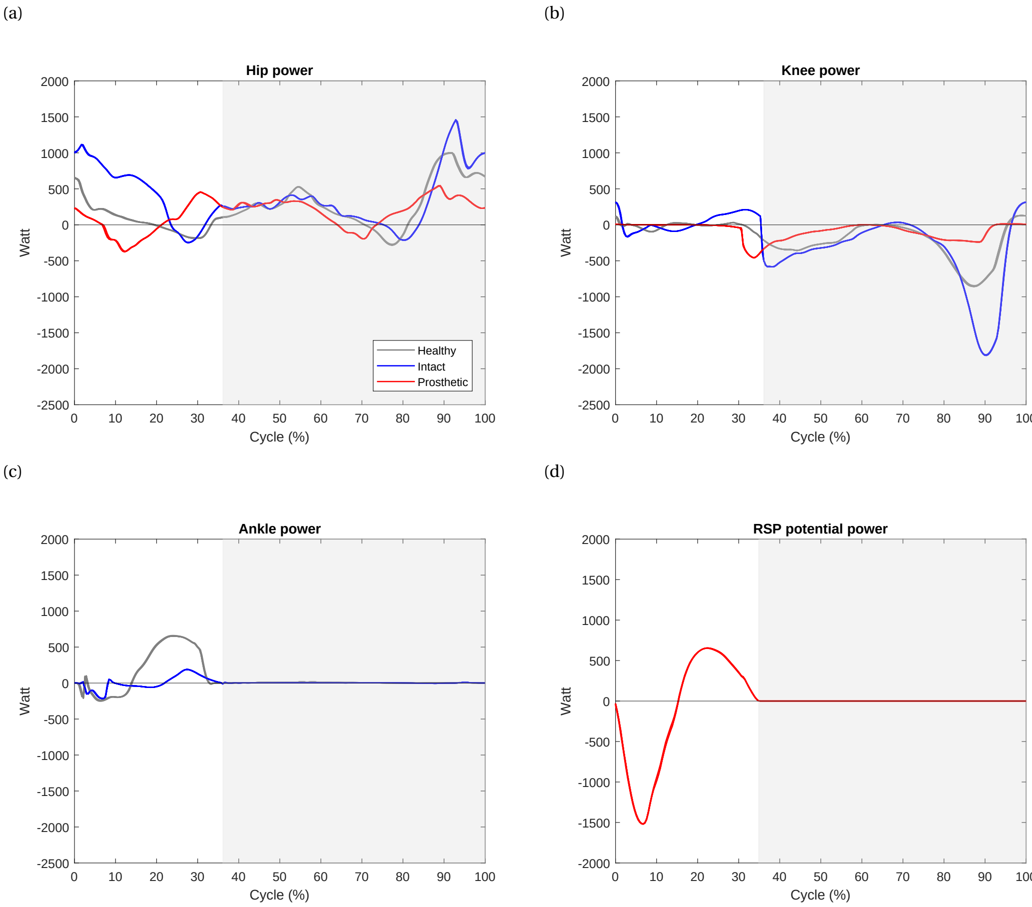

Figure 3.5: a) Hip, b) knee, c) ankle muscle power and d)RSP power generated by the healthy, intact and prosthetic legs normalized by the percentage of the cycle of each leg. Overall, the intact leg produced 32% more total power ($P_{\text{intact}}=P_{\text{hip}}+P_{\text{knee}}+P_{\text{ankle}}$) than the prosthetic leg ($P_{\text{prosthetic}}=P_{\text{hip}}+P_{\text{knee}}+P_{\text{RSP}}$), and 31% more than the healthy leg. On the other hand, the RSP made up the 39.6% of the total prosthetic leg power for running at 3.5 m/s.

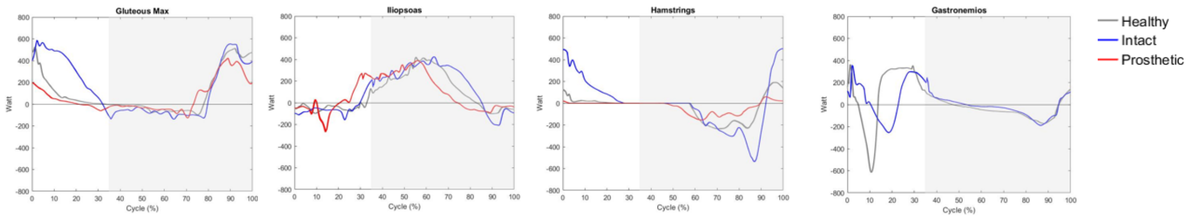

Figure 3.6: Individual muscles power of the Gluteus maximum, Iliopsoas, Hamstrings, and Vasti, of the healthy, intact and prosthetic leg by the percentage of the gait cycle. The muscles from the prosthetic leg could not generate as much power as the muscles from the healthy leg.

3.2. Effect of RSP stiffness on amputee's running biomechanics

After gaining knowledge about the basic biomechanics of an amputee subject, simulations for different RSP stiffness categories were performed in order to find the optimum stiffness for our specific athlete. The approach described in Section 2.2.2.C was followed to carry out the simulations. From softer to stiffer prosthesis categories, Cat4, Cat5, Cat6, Cat6High and Cat7 were chosen to be simulated. In this section, the main results concerning the differences in performance, motion, spatiotemporal variables, power generation and spring-mass leg mechanics for the different categories are posed.

A. Effect of RSP stiffness on running efficiency and maximum performance

Figure 3.7a illustrates the metabolic cost consumed wearing the different prosthesis models running at 4 m/s. The lowest metabolic cost happened when the amputee subject used the Cat6 RSP, which resulted to be the prescribed stiffness for its body weight. Metabolic cost expended to run 10 seconds at 4 m/s was 7.21, 7.29, 6.91, 6.93, 6.96 J/kg/m for Cat4, Cat5, Cat6, Cat6High and Cat7 stiffness categories respectively.

In addition, the maximum performance also differed between the simulations with different prosthesis. It can be observed in Figure 3.7b that the optimum was found for the model wearing the Cat6High RSP, achieving a maximum velocity of 4.675 m/s. Softer prosthesis accomplished decreasing maximum velocities, 4.62 m/s, 4.36 m/s and 4.27 m/s for Cat6, Cat5, Cat4 respectively. Stiffer prostheses also resulted in a slower maximum velocity of 4.55 m/s. Even though the difference in velocity did not seem significant, for running 200 metres or 400 metres it became important. For instance, using the Cat 6 High the model could achieve 200 metres 0.5 seconds before than when using Cat 6 (see, Table 3.1).

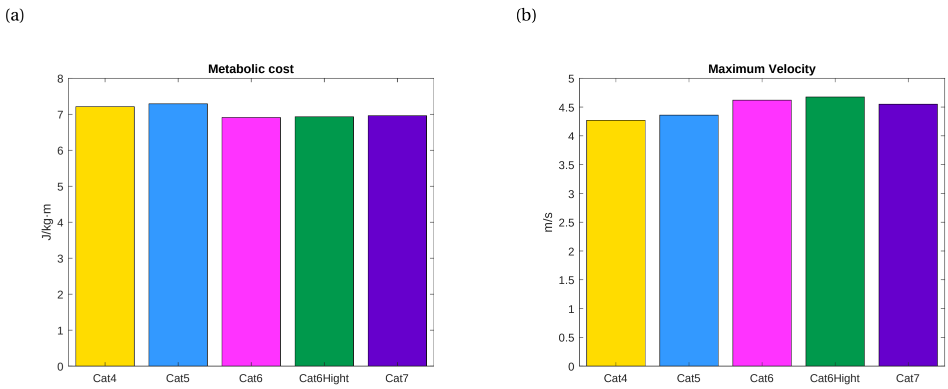

Figure 3.7: a) Metabolic cost consumed running at 4m/s for each stiffness category. Cat6 stiffness resulted in the lowest metabolic cost. b) Maximum velocity achieved by the model for each stiffness category. Maximum performance occurred when wearing Cat6High.

Stiffness category	200 m (s)	400 m (s)
4Low	46.8	93.7
5Low	45.8	91.7
6Low	43.3	86.6
6High-7Low	42.8	85.6
7High	43.9	87.9

Table 3.1: Times to run 200 m and 400 m that the model would achieve wearing each RSP category for running at maximum velocity.

B. Effect of RSP stiffness on motion

(a) **Intact** (b) **Prosthetic**

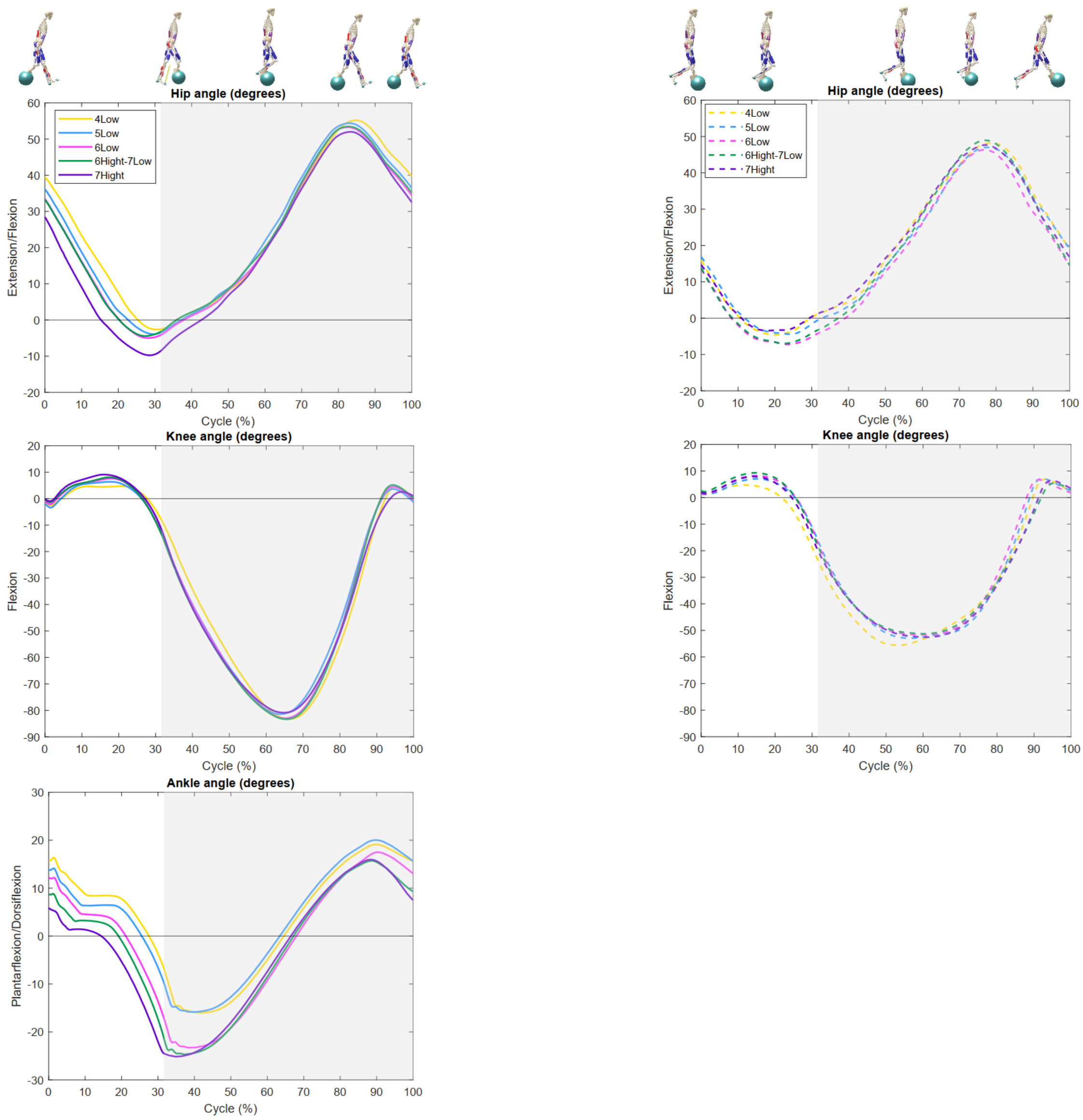

Figure 3.8: Effect of prosthesis stiffness on motion running at maximum velocity. Joint angles normalized by the gait cycle for the a) intact and b)prosthetic leg are shown for the five stiffness.

On the other hand, in Figure 3.8 the effect of the RSP stiffness in motion can be observed. The intact leg presented a slight adaptation on peak hip extension angles during contact for different stiffness, as stiffer the prosthesis was the intact leg displayed larger hip extension angles. The hip extension angles values were 2.6º, -3.9º, -4.9º, -4.4º, -9.7º for Cat4, Cat5, Cat6, Cat6High and Cat7 prosthesis respectively. Moreover, it appeared that the intact leg ankle also regulated notably the plantarflexion angle at the toe-off with prosthesis stiffness. Increasing stiffness was related to greater peak plantarflexion angle. The peak plantarflexion angles values were 14.6º, 14.54º, 21.4º, 23.7º and 25.2º for Cat4, Cat5, Cat6, Cat6High and Cat7 prosthesis respectively. By contrast, no notable effect of prosthesis stiffness was seen in hip and knee angles of the prosthetic leg.

C. Effect of RSP stiffness on spatiotemporal variables

Spatiotemporal variables from the simulations performed for different RSP stiffness running at maximum speed are given in Figure 3.9. Decreasing trends in stride and contact times for both intact and prosthetic legs were seen with stiffer prosthesis. Cat4 presented a stride time of 0.504s, Cat5 of 0.494s, Cat6 of 0.493s, Cat6High of 0.493s and Cat7 of 0.487s. Moreover, the intact legs had contact times of 0.172s, 0.164s, 0.161s, 0.158s, 0.154s, while prosthetic legs of 0.165s, 0.1597s, 0.146s, 0.139s, 0.138s for Cat4, Cat5, Cat6, Cat6High and Cat7 stiffness categories respectively. Furthermore, flight times of the intact legs were not correlated with stiffness (0.1132s, 0.1096s, 0.1248s, 0.1308s, 0.1272s for Cat4, Cat5, Cat6, Cat6High and Cat7 respectively). However, prosthetic legs showed an increasing trend in flight times with prosthetic stiffness (0.0560s, 0.0628s, 0.0632s, 0.0676s, 0.07s for Cat4, Cat5, Cat6, Cat6High and Cat7 respectively).

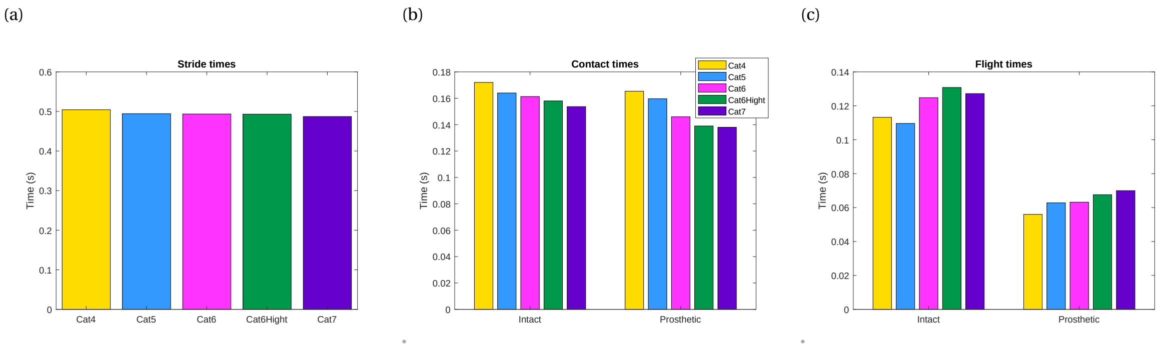

Figure 3.9: a) Stride times, b) contact times and c) flight times of both intact and prosthetic legs for wearing different prosthesis stiffness categories, when running at maximum speed.

D. Effect of RSP stiffness on power

Furthermore, a deep power analysis was performed to observed the adaptation of the model to the different stiffness. The intact leg total power was divided into the muscle power developed around the hip, knee and ankle joints, while the prosthetic leg total power consisted of the muscle power evolved around the hip and knee joints and the power exerted by the RSP. The instantaneous joints power normalized by the percentage of the cycle can be observed in Figure 3.10. Individual muscles power are displayed in Appendix C.

In **Figure 3.10** it can be observed that the hip muscles produced the majority of the power in the intact and prosthetic legs. Firstly, looking at the **intact leg** joints powers, the hip generated positive power to bring the leg underneath the trunk, at the touch-down and until the 20% of the stride. This power was mainly produced by the gluteus maximus and the hamstrings. During the same period of time, power was absorbed in the knee joint by the gastrocnemius muscle due to the impact of the touch-down. Secondly, just before the toe-off, there was absorption of power by the iliopsoas in the hip to break the extension of the hip, while the knee developed power by the gastrocnemius to start being flex. Thirdly, at the toe-of, the hip produced positive power with the iliopsoas to bring the leg forward until the middle of the stance phase of the other leg (about 70% of the stride). Meanwhile, the knee was being flexed by a passive motion that was broken by the vasti muscle at the beginning of the swing phase. Then, at the middle of the stance phase of the prosthetic leg, the rectus femoris generated positive power to start the extension of the knee, which was decelerated around the 90% of the stride by the hamstrings, during the prosthetic leg flight phase. Finally, when the leg was fully stretched forward, there was again generation of power by the gluteus maximus and the hamstrings in the hip and by the hamstrings and gastrocnemius at the knee, to start pulling the leg backwards before the touch-down.

On the other hand, the **prosthetic leg** presented a similar profile of joint powers than the intact leg, however, the power production was much lower. Especially, during the stance phase, the hip hardly generated power to bring the leg backwards. Moreover, it absorbed power about the 12% of the stride, mainly by the iliopsoas. This coincided with the moment that the RSP started releasing the power stored. Furthermore, the knee barely developed power during the whole stride. Only the rectus femoris and vasti produced power around the 60% of the stride in order to start the extension of the knee just before the toe-off of the intact leg. Afterwards, the extension of the knee was broken around the 90% by the hamstrings, however, the absorption of power was much less than in the intact leg. This was related to the reduced weight of the shank in the prosthetic leg. In addition, regarding the RSP, it released most of the power around the 15%, while the intact ankle around the 25%.

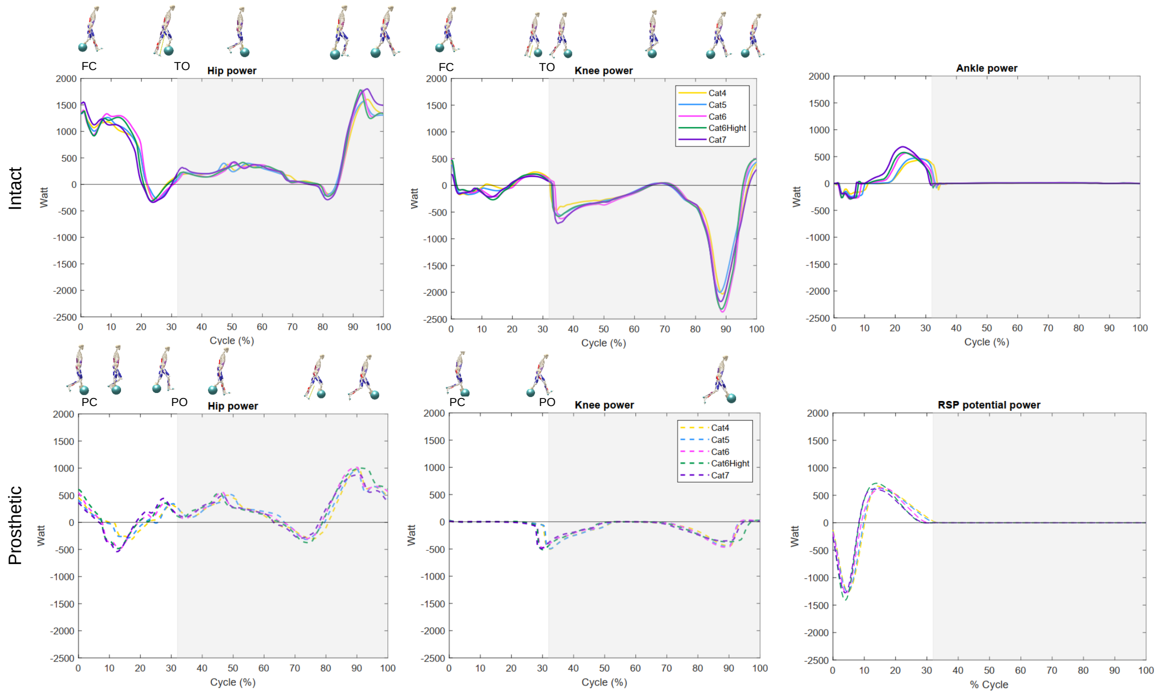

Figure 3.10: Muscle power developed around the hip, knee and ankle joints in the intact leg and power developed by the hip joint, knee joint and the RSP in prosthetic leg, for every RSP category. FC regards to foot-contact, TO to toe-off, PC to prosthesis contact and PO to prosthesis-off.

In order to compare the performance for different RSP, the average positive and negative powers per cycle were computed for the intact and the prosthetic legs of every RSP configuration and were collected in **Table 3.2**. On the one hand, it was observed that the positive hip power in the **intact leg** did not correlate with performance or stiffness, however, it was seen that stiffer RSPs exerted higher power than softer prostheses. Moreover, the positive intact knee power was highest for Cat 6 High and the power absorbed at the intact hip and knee increased for the stiffness category. Increasing positive power was also developed around the ankle with RSP category.

On the other hand, the **prosthetic leg** showed modulation in the hip positive power, which was correlated with the performance. The Cat 6 High allowed exerting more hip power than the other configurations. This power was specially modulated by the gluteus maximus during the contact phase (see, Appendix). Besides, the knee positive power was insignificant compare with the hip power and barely differed between prosthesis stiffness. Furthermore, the absorption of power at the knee joint was related to the velocity of the model. For faster speeds, greater power was absorbed in the knee joint. Additionally, regarding the RSP power, decreasing positive power happened as stiffer the prosthesis was, except for Cat6High, which released more power than the Cat6. Remarkably, the RSPs released almost all the energy stored. Further analysis of the energy stored, released and lost of each RSPs over a cycle is presented in Appendix D.

	Intact leg						Prosthetic leg						TOTAL	
	Hip		Knee		Ankle		Hip		Knee		RSP			
Stiffness	P+	P-	P+	P-	P+	P-	P+	P-	P+	P-	P+	P-	P+	P-
Cat4	5.07	0.29	0.54	3.19	0.58	0.22	2.41	0.56	0.03	1.11	1.00	1.01	9.65	4.37
Cat5	5.11	0.33	0.57	3.38	0.60	0.21	2.48	0.51	0.03	1.13	0.99	1.00	9.78	4.58
Cat6	5.34	0.35	0.57	3.80	0.76	0.27	2.71	0.61	0.04	1.15	0.95	0.95	10.37	5.23
Cat6High	5.20	0.36	0.66	3.80	0.77	0.22	2.91	0.73	0.03	1.20	0.97	0.97	10.54	5.34
Cat7	5.40	0.45	0.46	3.87	0.92	0.16	2.63	0.70	0.02	1.13	0.87	0.87	10.29	5.45

Table 3.2: Average positive (P+) and negative (P-) power in W/kg developed by the intact and prosthetic leg in a gait cycle for each stiffness category. Average power were computed as energy divided by the stride time. Each leg was split in its different sources of power: P_{intact}=P_{hip}+P_{knee}+P_{ankle} and $P_{\text{prosthetic}}$=P_{hip}+P_{knee}+P_{RSP}. The TOTAL power is the sum of the intact and prosthetic leg.

Moreover, as a summary of the power generated in time, Figure 3.11 shows the intact and prosthetic legs average total positive power. Overall, the intact legs could generate more average power than the prosthetic legs. Particularly, Cat 6 High presented less asymmetry in power generation between legs. The prosthetic leg produced 58.9% of the total intact leg power. From the total prosthetic leg power, the RSP made up 24.8% while the muscles 75.2%.

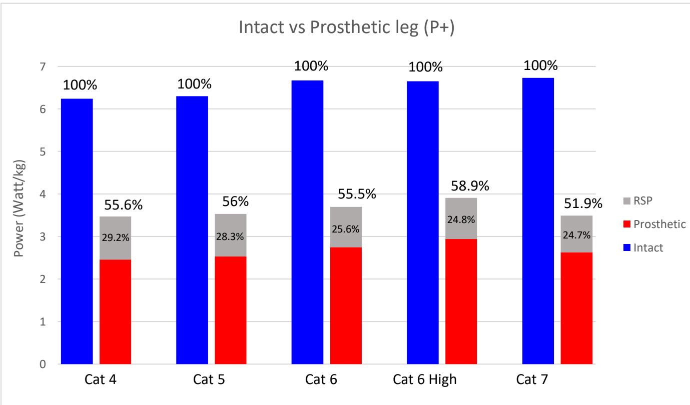

Figure 3.11: Average positive power (P+) of the intact (blue) and prosthetic leg (red regards muscles + grey regards RSP) for each stiffness category. It was observed that if the intact legs made up the maximum power (100%), the total power of the prosthetic legs (muscles+RSP) corresponded to 55.6%, 56%, 55.5%, 58.9% and 51.9% of the intact legs power, for Cat 4, Cat 5, Cat 6, Cat 6 High and Cat 7 respectively. Thereby, Cat 6 High had more prosthetic leg total power and smaller asymmetry between legs in power generation than the others categories. Moreover, the percentage of the RSP power in the total prosthetic legs powers can be seen in the graphs (grey areas).

E. Effect of RSP on Spring-mass leg mechanics

In order to have a better understanding of the spring-mass behaviour of the total legs, leg stiffness (K_{leg}) was computed following the approach described in Section 2.4. Increasing K_{leg} was observed with stiffness for both intact and prosthetic legs (see, Figure 3.12.a). Regarding the Cat4, Cat6, Cat6High and Cat7 intact legs K_{leg}, they were 5.8%, 10.4%, 14.3%, 2.9% lower than the corresponding prosthetic leg K_{leg}. While for Cat5 intact leg K_{leg} was 2.3% greater than the prosthetic leg.

Besides, GRF versus vertical CoM displacement hysteresis curves of both legs for every RSP configuration is illustrated in Figure 3.12.b and c. In addition, Table **??** collects the energy stored, generated and hysteresis of the intact and the prosthetic legs. Comparing intact and prosthetic legs, the intact ones generated significantly more energy, while stored meaningless energy compared with the prosthetic legs. Nonetheless, all the energy generated in the intact legs was lost while the prosthetic legs recoiled partially the energy stored.

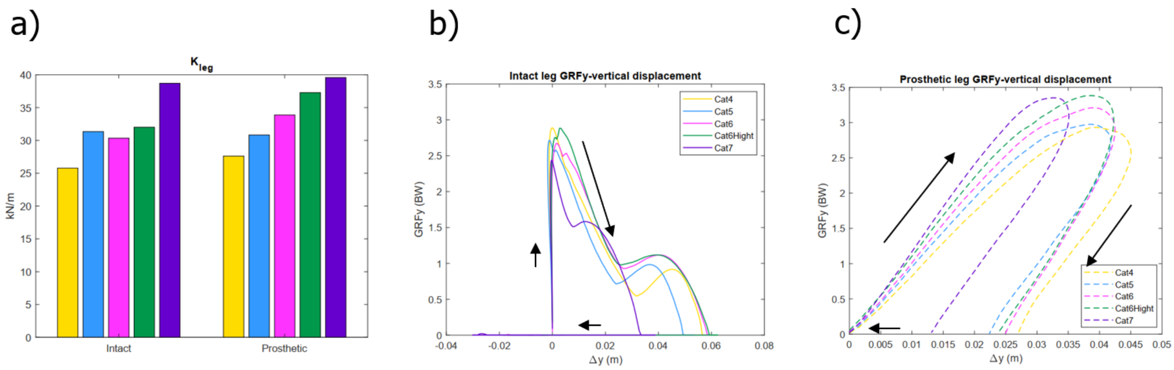

Figure 3.12: a) Legs' stiffness (K_{leg}), GRF-vertical displacement curves of the b) intact and c) prosthetic legs for each RSP stiffness. The prosthetic K_{leg} was greater than the prosthetic K_{leg} for every prosthesis configuration except for Cat5. Moreover, it is seen that the intact leg lost all the energy that generated, while the prosthetic leg had recoil.

	Intact leg				**Prosthetic leg**				
Stiffness Category	**E stored (J)**	**E generated (J)**	**Hyst (J)**	**Recoil (%)**	**E stored (J)**	**E generated (J)**	**Hyst (J)**	**Recoil (%)**	**Total E generated (J)**
Cat4	1.08	60.48	59.39	2	60.74	11.48	49.26	18.9	71.95
Cat5	1.87	55.86	53.99	3	58.00	16.36	41.63	28.22	72.23
Cat6	1.21	68.21	67.00	2	64.78	13.46	51.32	20.78	81.67
Cat6High	0.16	70.32	70.16	2	67.34	16.55	50.78	24.58	86.87
Cat7	2.28	54.08	51.80	4	59.76	20.79	38.97	34.78	74.87

Table 3.3: Energy stored, generated, hysteresis (Hyst) and recoil of the intact and prosthetic legs during a gait cycle for each stiffness category. Total E generated regards the sum of the E generated by the intact and the prosthetic leg.

3.3. Accuracy of the simulations

Due to the lack of experimental data, two main articles from the literature were selected to compare and assess our simulation accuracy. First, Sepp et al [26] provided the kinematic data of able-bodies and amputee athletes wearing RSP running at 3.5 m/s. Second, Beck et al [5] analyzed the spatiotemporal variables and GRFs peaks of an elite amputee sprinter running in a treadmill for a range of velocities (2.8 to 11.55 m/s). The approach followed to perform the simulations required for these comparisons is described in Section 2.2.2.D.

Joint angles

Figure 3.13 shows the differences between the simulation and the experimental data in the hip and knee angles of the healthy, intact and prosthetic legs. On the one hand, it can be observed that the simulation results presented lower peak hip extension angles than the data reported by Sepp et al [26]. Specifically, they were 11.4º, 10º and 5.6º smaller in the healthy, intact and prosthetic legs respectively. Moreover, peak hip flexion angles were higher in the simulation than in the experimental data by 19º, 9º and 4º in the healthy, intact and prosthetic legs respectively. On the other hand, peak knee flexion angles resulted to be inferior in the simulations, 9.6º smaller in the healthy leg, 15.6º in the intact leg and 28.4º in the prosthetic leg. In addition, knee joints presented hyperextension on the simulations, which was not measured in the real data. The healthy and intact legs revealed a 7.3º knee hyperextension angle while the prosthetic leg displayed 13º.

Besides, some similar trends in peak angles between legs are seen in the experimental data with our simulations. First, greater peak hip extension was seen in the healthy leg with respect to the intact leg in both experimental and simulation data. Moreover, the peak hip flexion angle was also smaller in the prosthetic leg than in the intact leg in the simulation. Lastly, the correlation between trends in the peak knee angles is also observed between literature and the simulation. The intact leg presented the highest peak knee flexion while the prosthetic leg showed the lowest. Nevertheless, not comparable trends were identified between healthy and intact peak hip flexion and prosthetic and intact peak hip extension.

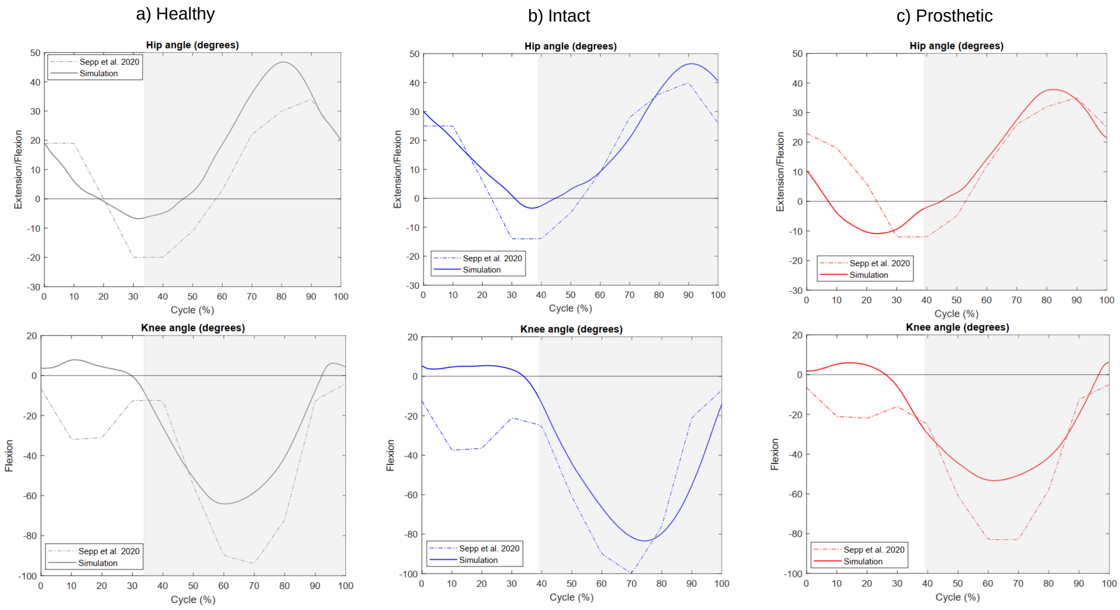

Figure 3.13: Accuracy of the simulation in the joint angles. a) Healthy, b) intact and c) prosthetic legs' hip and knee angles over the percentage of the gait cycle. Dashed lines represent the experimental data from Sepp et al [26] and solid lines the simulation results. The grey area represents the swing phase of the gait cycle.

Adaptation to running velocity

As it was mentioned before, Beck et al [5] aimed to analyze the adaptation of amputee athletes to different running speeds. For that purpose, they quantified spatiotemporal variables and peak ground reaction forces over a range of speeds of the world record amputee sprinter using RSP. This information was used to observe if our model would adapt its biomechanics the same way as a human.

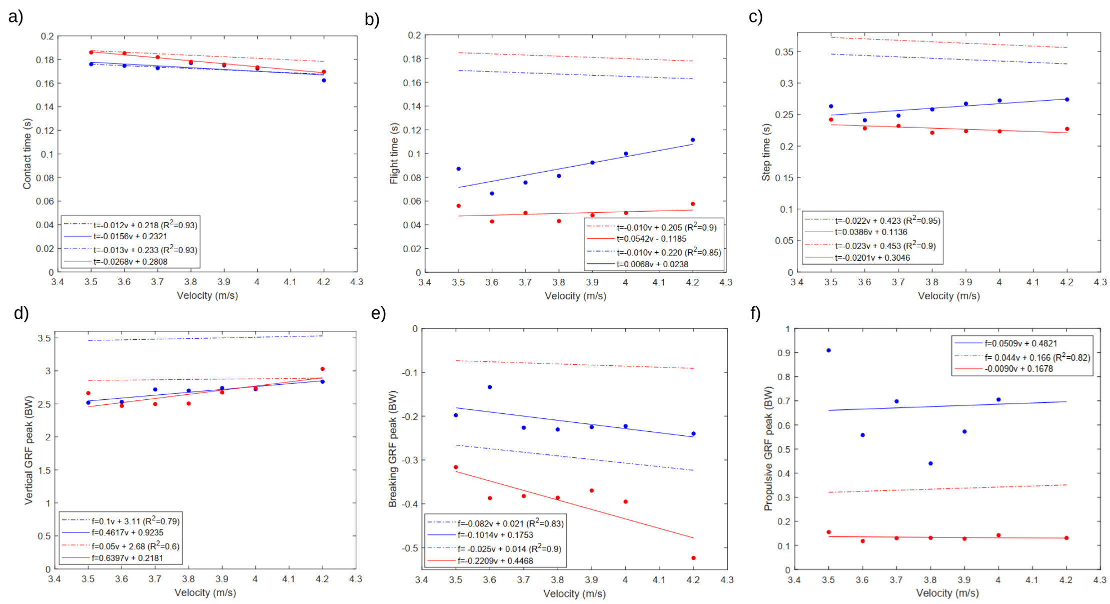

Figure 3.14: Comparison between experimental data collected by Beck et al [5] (dashed lines) and simulation results (solid lines). The blue lines correspond to the variables of the intact leg and the red lines of the prosthetic leg. The dots are the simulation results. a) Contact times, b) flight times, c) step times, d) vertical GRF peaks, e) breaking GRF peaks and f) propulsive GRF peaks over a range of velocities (3.5 to 4.2 m/s) regression lines are presented.

The most remarkable difference between the athlete and our model was the maximum speed accomplished. The human could reach 11.55 m/s, which was the maximum speed of the treadmill, while the model could only get to 4.2 m/s. However, there were some similarities in the variables' trends over the range of speed. The model and the experimental data were compared for the same range of velocities. Figure 3.14 illustrates the regression lines of the experimental data and the simulation results of contact time, flight time, step time, GRF vertical peak and GRF propulsive and breaking peaks. Both contact times of the intact and the prosthetic legs decreased with speed with similar slopes, although the simulation appeared to have steeper trends (see, Figure3.14.a). Prosthetic leg step time also showed a comparable trend that the one reported in the study, however, the times were about 1.5 shorter in the simulation (see, Figure3.14.c). However, no correlations between trends were observed in flight times and intact leg step time. Moreover, vertical GRF peaks resulted in increasing tendency in both legs in the simulation and the measurements, still, the slopes were more abrupt in the model. Additionally, like in the experimental results, simulations displayed a decrease in break GRF peaks with speed for both legs. Prosthetic propulsive GRF peaks showed comparable values with the measured values. Intact propulsive GRFs peak regression line appeared not to be related to speed in both experiment and simulation.

Concluding this section, the results from the simulations are discussed in the following chapter. There, we analyze how reliable the simulations are and if they are comparable with reality.

4 Discussion

In this chapter, the research questions raised in the introduction are discussed based on the knowledge obtained from the simulation results. Moreover, at the end of this chapter, the accuracy of the simulations are examined.

4.1. Is it an asymmetric running pattern optimal for unilateral transtibial amputees?

Yes, it is. As it was expected, due to the differences in muscle mass between legs and missing the ankle joint in one leg, asymmetric biomechanics evolved from the simulations of the unilateral runner, in terms of kinematics, spatiotemporal variables, GFRs and leg muscle power.

First, asymmetry in joint angles was observed between the intact and the prosthetic leg. Particularly, a significant difference in the knee flexion during the swing phase was seen. The intact leg presented a greater angle than the prosthetic and the healthy legs. This was caused due to the higher negative vertical displacement of the CoM during the prosthesis stance phase, compares with the small vertical displacement that occurred during the intact leg stance phase. The intact leg needed larger knee flexion to bring the leg forward. Understandably, the prosthesis height plays an important role in the difference of the CoM vertical displacement between legs during contact. In the model, the prosthesis was set to be 3 cm longer than the intact leg, which was in the range that is normally recommended, regardless of the RSP stiffness. However, this parameter should be optimized depending on the RSP stiffness, to compensate for the deflection of the prosthesis and keep the total leg length as similar as possible to the intact leg.

Second, regarding the spatiotemporal variables, the prosthetic leg showed shorter contact time than the intact leg. Considering that the total leg stiffness is lower in the prosthetic leg, the contact time should have been larger in the prosthetic leg than in the intact leg. This result might be associated with the damping coefficient and the impedance set for the joint that connected the socket and the amputated tibia. In reality, is expected that a loss of energy occurs at this connection as it is not a weld joint. On the contrary, in the model, the vertical stiffness parameters of the socket joint were set to the same values as the rest of the body joints, which might not be realistic. To our knowledge, no study calculated the damping at the socket-tibia interface.

Third, ground reaction forces peaks also differed between legs, especially in the x-direction. A lower propulsive force peak was observed in the prosthetic leg. This restricts the forward acceleration of the athlete while running, which is a clear disadvantage of the prosthetic leg. Unlike the RSP, which has a fixed stiffness, the muscles of the ankle joint are able to change stiffness when required. This permits giving the power at the right moment during the take-off when the CoM of the athlete is farthest from the centre of pressure and the force is more horizontally oriented. Nevertheless, the contact point where the force is applied and the shape of the blade are key to drive the body of the athlete in a more forward than vertical direction during the contact of the prosthesis. A greater plantarflexion angle of the prosthesis would make the point of pressure closer to the tip of the blade, pointing the force in a more horizontal direction, but there is a trade-off between balance and the alignment angle in the sagittal plane.

Lastly, regarding the power balance, the most remarkable finding was observed in the difference in muscle power between legs. As a result of missing the muscles around the ankle joint as well as not being able to exert much power with the gluteus, hamstrings and iliopsoas muscles, the prosthetic leg developed 32% less power than the intact leg. To compensate for this, the intact leg needed to generate 31% more muscle power than the healthy leg to run at the same velocity.Besides, the hip produced most of the muscle power. Particularly, during the first part of the stance phase the crucial muscles that exerted the force to the ground to bring the leg backwards were the gluteus maximus and hamstrings in the intact leg and just the gluteus in the prosthetic leg. During the second part of the stance phase, just before the puss-off, mainly the gastrocnemius and soleus developed the power in the intact leg and the RSP in the prosthetic leg to propel the body into the flight phase.

Remarkably, high-frequency oscillations occurred in the muscles length and therefore the individual muscle powers were affected. These oscillations occurred due to the low stiffness and damping properties established for the cartilage model between the joints, which provoked small vibrations of the segments. Nevertheless, the overall results were not affected.

It is important to mention that in our model the muscle mass was equally distributed in both legs which might not be a good approximation to reality. Amputees could develop more muscle mass in one leg than in the other one to compensate for their impairment. However, no data about muscle mass in amputees was available in the literature.

4.2. What is the effect of prosthesis stiffness on running economy and performance?

It was observed that adjusting the prosthesis stiffness influenced the running economy and performance of the model. The model consumed the least metabolic cost wearing the stiffness category prescribed for its body weight (Cat6). Moreover, it seemed that softer RSP required more metabolic energy than the stiffer ones to run at the same velocity. This could be related to the longer contact times in the prosthetic leg. Uchita [29] metabolic cost model is dependable on the amount of time the muscles are exited above 10%. As the muscles, especially the gluteus maximus (see, Appendix E), were stimulated for a longer time during the contact the metabolic cost increased. However, to investigate this, it would be needed to observe every muscle excitation function.Furthermore, stiffer RSP than Cat 6 caused a comparable metabolic cost to run at the same velocity. In reality, it appears that stiffer prostheses increase the heart rate of amputees while running [11]. This might be an important factor to take into account for long-distance running, however, this was not considered in our model.

On the other hand, category Cat6High performed the best achieving the fastest speed the model could achieve. This greater performance is related to an optimal adaption of the athlete to the stiffness of the prosthesis. Despite the athlete accomplished similar velocities with all prosthesis, the difference for running 200 metres became important, as there was a deviation of 0.5 seconds between Cat6High and Cat6.
Nevertheless, the motion was optimized for a steady-state running when the performance during the acceleration phase is crucial, especially in a 100-m sprint. But still, our results could be used for an initial guess of the possible optimal combination athlete-prosthesis.

Concluding, we could learn from the simulations that a prescribed stiffness Cat6 category would allow our model to perform better in long-distance races, but when sprinting, the runner would probably achieve faster velocity using Cat6High.

4.3. What is the effect of prosthesis stiffness on motion and the running cycle?

Mild adaptations in the motion pattern of the intact leg were observed due to adjusting the prosthesis stiffness. Especially, at the touch-down, a decreased in ankle dorsiflexion angle and intact leg hip flexion were observed with stiffer prosthesis. This was related to a higher CoM position during the flight phase of the prosthetic leg for stiffer categories (see, Appendix B). As higher the CoM was at the landing of the intact leg the

hip was less flexed. This was associated as well with an increased ankle plantarflexion and intact leg hip extension angles with stiffer blades at the take-off. Due to landing with lower hip flexion and lower dorsiflexion angle, both joints could rotate to larger ankle plantarflexion and hip extension angles more effectively during the contact. This allowed a better push off of the intact leg and longer flight times for stiffer blades. Cat6High presented the longest intact leg fight time.
Furthermore, the model also adapted its intact and prosthetic leg contact times depending on the prosthesis stiffness. Decreasing trends with stiffness category were shown in both legs, this is related to lower stiffness of the total legs. In the prosthetic leg, the total leg stiffness is governed by the prosthesis stiffness, while in the intact leg by the tendons' stiffness. Stiffer prosthesis and tendons stretch and recoil quickly and more effectively under large forces, thereby, the transfer of force from the prosthesis/muscles to the skeleton is quicker, which concludes in reduced ground contact time.

4.4. What is the effect of prosthesis stiffness on power generation during the cycle?

It was observed that the model was able to module the muscle power exerted to the prosthesis and could use the intact leg more effectively depending on the RSP category used.

Certainly, the performance of the athlete was related to the muscle power exerted by the **prosthetic leg** to the RSP. The model was capable to adapt the power at the prosthetic hip and knee joints and make the muscles stiffer when using Cat6High. Even though softer prosthesis stored and returned more energy, the athlete could not generate as much power with its prosthetic leg muscles, thereby the performance was inferior. Particularly, the athlete was capable of generating more power with the gluteus maximus for extending the hip just before the touch-down and during contact. This allowed to stored greater energy in the Cat6High RSP than in Cat6 RSP. However, the prosthetic gluteus could not pull the leg back as much as the intact legs during the contact. Moreover, the iliopsoas started to break the extension of the hip just at the GRF peak to control the leg when the energy is released by the prosthesis and avoiding rolling over the RSP too fast and fell forward.

In addition, the **intact legs** also benefited from the optimal use of the prosthetic leg when using stiffer RSP. They exerted higher power and made the total leg stiffer. This phenomenon was related to the larger extension at the hip and ankle plantarflexion during the contact phase. This allowed to generated higher power with the ankle at the push-off, especially with the soleus muscle, and propel the body to longer flight times.

Furthermore, the asymmetry between legs was analysed in Figure 3.11. The RSP could not compensate for the difference in muscle power between legs. It was observed that the RSP produced comparable power to the ankle joint of the intact leg and it made up 24.8% of the total prosthetic power using the Cat6High. Nevertheless, the athlete was not able to make the leg as stiff as the intact leg with the muscles, so the total power delivered by the prosthetic leg was lower. Particularly, using the Cat6High the intact leg produced 41% more power than the prosthetic leg, including the RSP. Therefore, it can be deduced that the RSP does not empower the amputee runner over able-bodies.
Moreover, it can also be observed from the hysteresis loop of both legs that the intact legs stored insignificant energy compared with the prosthetic legs and the recoil was almost none. This is because the muscle structure does not allow to store energy unlike the prosthesis, and all the energy generated was lost. This is a disadvantage from the intact leg.

4.5. How accurate are the simulations?

Overall, the simulations could resemble reality reasonably in terms of motion, times and forces. Nevertheless, larger differences in velocity.

Regarding the motion, peaks angles occurred at similar moments in times and followed comparable trends between legs than in the experimental data. However, the model underestimated hip extension angles and knee flexion angles, while hip flexion angles were generally higher in the simulations. These variations could be caused due to the little experience in running that the subjects from Sepp et al study had. The model chose the most optimal motion which was keeping the foot/prosthesis as close as possible to the floor during the swing phases, but humans are more aware of falling than the model, so they might use more flexion of the hips and the knees during the swing phase. Moreover, Sepp et al did not specify which prosthesis models and setup, such as stiffness and height, were used by the subjects, which might have influenced the results as well. On the other hand, hyperflexion of the knee occurred during the contact of all the limbs in the simulations. Comparing with the real data, which shows a small flexion of the knee during the contact, the model run with very stiff legs with the knee completely stretched. This might be a result of the low joint limit stiffness set for the ligaments model. The reference model has been used for waking and this parameter may need to be adjusted for running gait, as the forces applied at the knee are higher. Moreover, another reason could be that the model does not feel the impact forces and therefore do not need to flex the knee to avoid injuries.

Furthermore, our model simulated highly precise contact times of the intact and prosthetic legs for a range of velocities presented in Beck et al [5] study. Therefore, it could be deducted that the Hunt-Cross Ley model resembled adequately the deformation, energy stored and released of the prosthesis while running. Nevertheless, it seemed that for higher velocities the difference between the experimental data and the simulation in the prosthesis contact time increased. Even though it is a small variation, it could be significant for elite velocities.

On the other hand, GRFs peaks followed similar trends with velocity but the values slightly differ. Vertical GRFs peak of the intact leg was significantly higher in the experimental data than in the simulation. This difference is probably caused due to the damping coefficient of the running shoe in the model. This value was guessed and might be different from reality. In addition, even though the bodyweight of the model was matched to the athlete characteristics, it might be possible that the athlete had greater muscle mass, and therefore applied higher peak force. Besides, the breaking GRF peak of the prosthetic leg was underestimated in the simulations. This might be related to the shape of the prosthesis and its stiffness in the x-direction. The RSP that Beck et al's athlete used was different from our model. Moreover, in our model, the shape was simplified by a sphere with the same stiffness regardless of the pressure point. In reality, the blade has different stiffness depending on the force point of application and on the prosthesis shape. Therefore, it seems that our model might not represent quite accurately the x-direction stiffness of the blade, due to the simplicity of the shape.

Furthermore, the impedance in the residual limb/socket interface also could influence the contact and flight times and the GRF peaks. Energy dissipation probably occurs at the socket connection but to our knowledge, no study has quantified the mechanical behaviour of the residual limb and socket junction while running.

5

Conclusions and Future Prospects

The primary aim of this thesis was to develop a UTT amputee musculoskeletal model wearing a RSP and optimize the motion for running at a certain speed. This was successful, the model was able to mimic the running behaviour of an amputee athlete and the power balance equation was verified. An asymmetric running bio-mechanics between legs evolved from the simulation in terms of motion, spatiotemporal variables, GRFs and leg muscle power. In the intact leg, the main power production was developed by the hip during the contact phase to push the leg backwards. However, due to missing the muscles of the ankle joint in the prosthetic leg and not being able to generate as much power by the hip muscle, the total muscle power was lower in the prosthetic leg.

As a secondary aim, finding the optimal athlete-RSP stiffness combination was wished, to achieve the best performance. Five different stiffness categories for the prosthesis were simulated until reaching their maximum velocity. It appeared that the Cat6High RSP enhanced the performance of the model. Different adaptations of both intact and prosthetic leg to the prosthesis stiffness were remarkable to achieve improved performance. Firstly, the model was able to adapt the prosthetic leg muscle power for the different stiffness categories. The Cat6High RSP allowed the athlete to generate the highest muscle power at the hip and therefore to store and release more energy in the prosthesis than the Cat6. Specifically, the Cat6High prosthetic leg could produce 11.8%, 10.1%, 5.4% and 10% more total power over a stride than when using Cat4, Cat5, Cat6 and Cat7 respectively. Secondly, the correct use of the Cat6High RSP enhanced the prosthetic leg to propel the body in a longer flight time with a CoM position higher than softer RSP. This allowed an optimal intact leg landing with a more favourable hip flexion and dorsiflexion ankle angles to be able to pull the leg backwards more powerful and exert the ankle power at the right moment for a better push-off of the intact leg. This was also beneficial to decrease the intact leg contact times and increase the total leg stiffness. Lastly, the model could not generate as much power with the prosthetic legs as with the intact legs. It showed that the prosthetic leg generated 44.4%, 44%, 44.5%, 41.2% and 48.1% lower total power, including the RSP power, than the intact leg when using Cat4, Cat5, Cat6, Cat6High and Cat7 respectively. The majority of the prosthetic leg power was due to the muscles rather than the RSP. Especially, the reduction of power comparing with the intact leg was observed during the contact phase by the gluteus maximus and hamstrings to extend the hip for the push-off.

The third aim was to validate the accuracy of the results with experimental data found in the literature. The model was able to resemble the running motion realistically. Moreover, it was capable of simulating the intact and prosthetic leg contact times across a range of speed quite accurate, especially for low velocities. It could be concluded that the Hunt-Cross Ley model resembled the deformation of the RSP reasonable. However, the impedance at the residual limb/socket interface had possibly a great influence on the GRFs results. Besides, the greatest shortcoming was that the maximum speed achieved by the model was far from what humans are capable of. This was on account of some limitation of the study:

- The model used was very simplified. It had just 21 muscles in the lower body and had fewer segments in the foot. Moreover, it did not include arms, which are essential for adding power while running.
- It was a planar model, therefore the power added to the movement due to the rotation of the torso was missing.

- The running gait controller was a simple spinal control.

Concluding, the goals of this master thesis project have been successfully reached. Even though the top speed of the model was not realistic, the motion and kinetic data were comparable for low running speed. Therefore, it could be presumed that a reasonable prediction of the optimal RSP stiffness for running about 4.6 m/s was achieved. The biomechanical model developed could potentially be used to assist coaches and athletes to have a better idea of the most suitable RSP stiffness. However, it is unknown if humans have the same capability of adapting to the prosthesis as the model.

As a follow-up to the conclusions and to increase the truthfulness of the simulations in the near future, we suggest the following:

- Improving the stiffness and damping terms at the joints of the musculoskeletal model, in order to prevent oscillations of the bodies and muscles.
- Precisely measuring the impedance at the residual limb/socket interface as well as the RSP damping.
- Adding more muscles in the legs and the upper body.
- Adding arms as well as more segments in the foot.
- Making a 3D model, to add the rotation of the torso and observe the mediolateral forces and balance of unilateral transtibial amputees with different RSP setups.
- Adjusting the prosthesis height regarding the RSP stiffness.
- Perform a further validation of joint moments and joint powers through inverse dynamic simulation with real measurements with the same RSP models.

A

Power balance

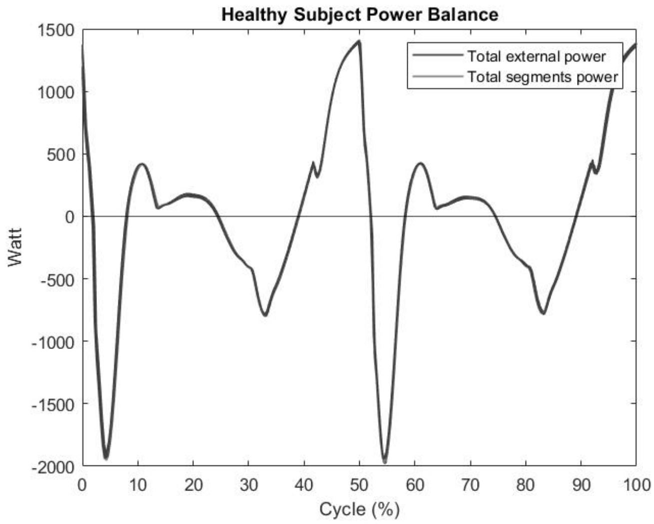

Figure A.1: Power balance of the healthy subjects by percentage of the gait cycle. Total external power = Total segments power

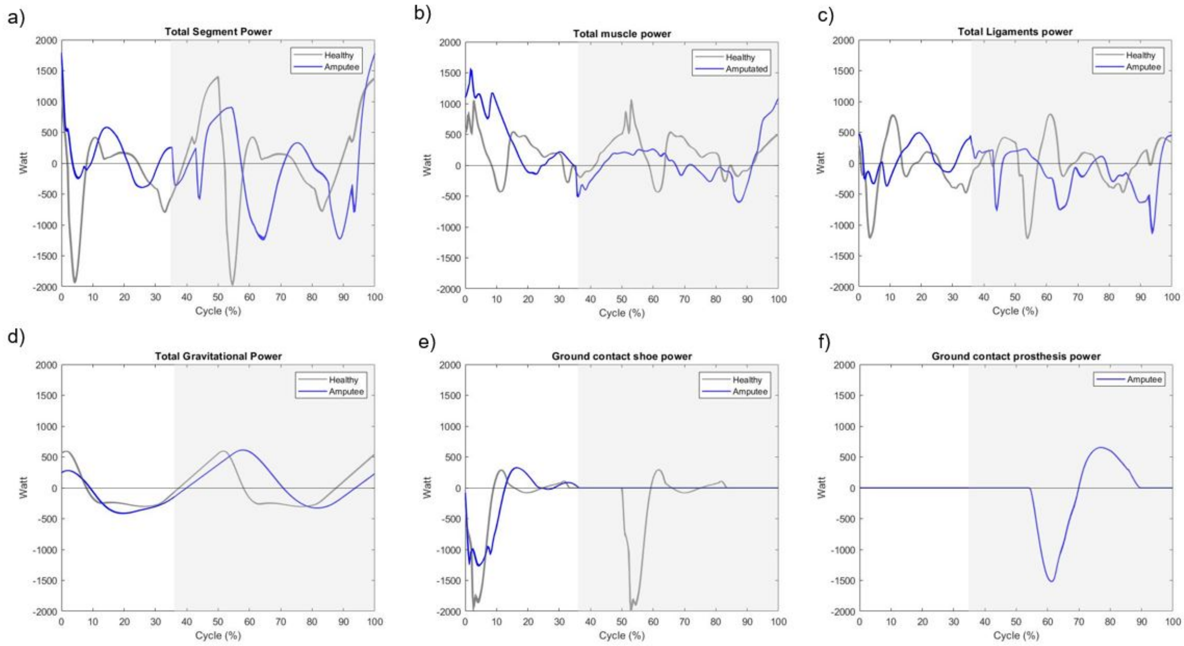

Figure A.2: Comparison of the different power sources that contribute to the total system power by percentage of the gait cycle for the healthy and amputee subject. a) Total kinetic segment power = total system power, b) total muscle power, c) total ligaments power, d) total gravitational power, e) ground contact shoe power and f) ground contact prosthesis power.

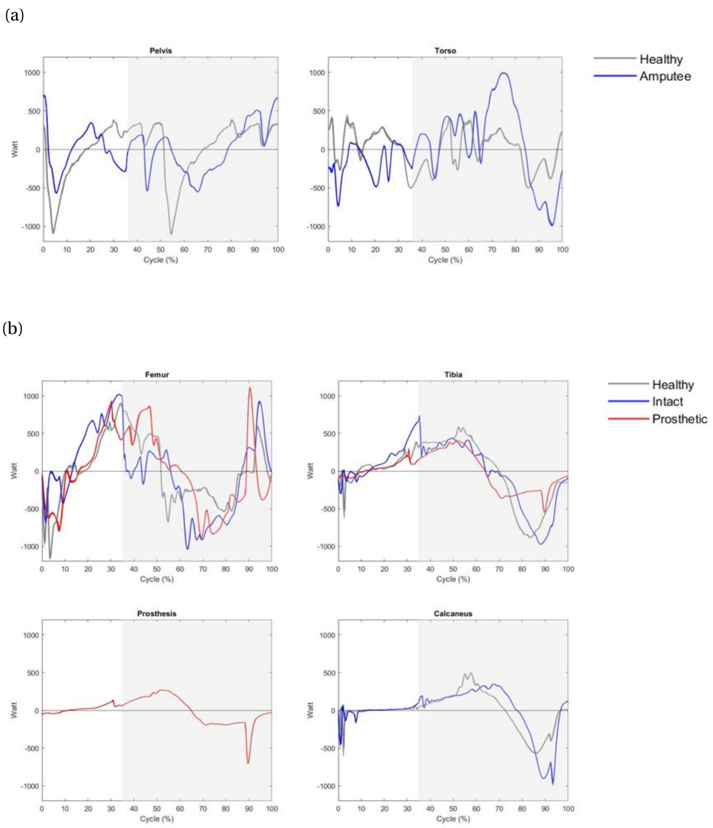

Figure A.3: Individual segments power comparison between the healthy and the amputee subject by percentage of the gait cycle. a) Pelvis and torso kinetic power of the healthy and amputee, b) femur, tibia, prosthesis and calcaneus kinetic power of the healthy, intact and prosthetic legs.

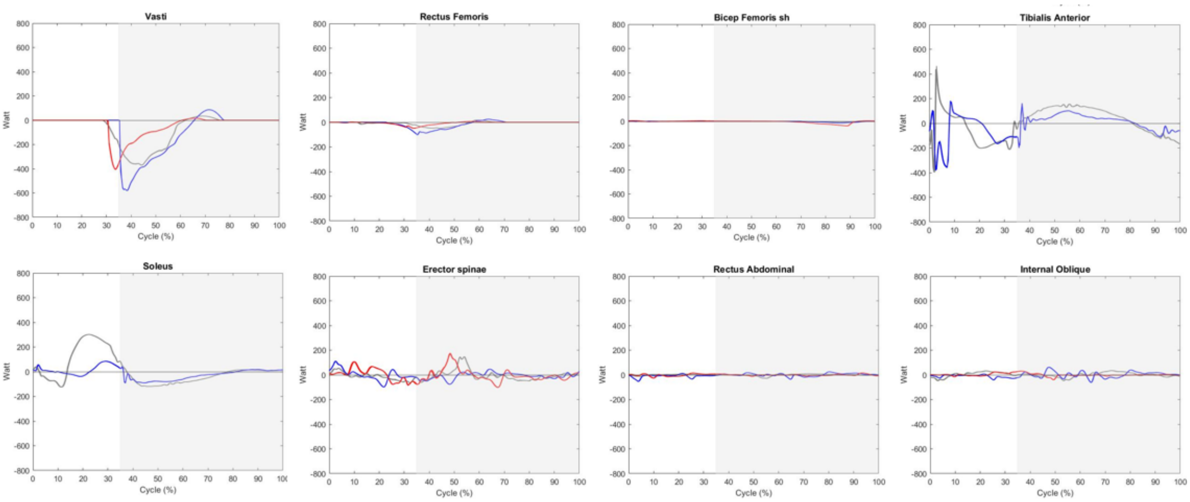

Figure A.4: Individual muscles power of the healthy (grey), intact (blue) and prosthetic (red) legs by percentage of the gait cycle. Bicep femoris short head,Rectus femoris, Gastronemios, Tibialis anterior, soleus, Erector spinae, Rectus abdominal and Internal oblique.

B
Motion

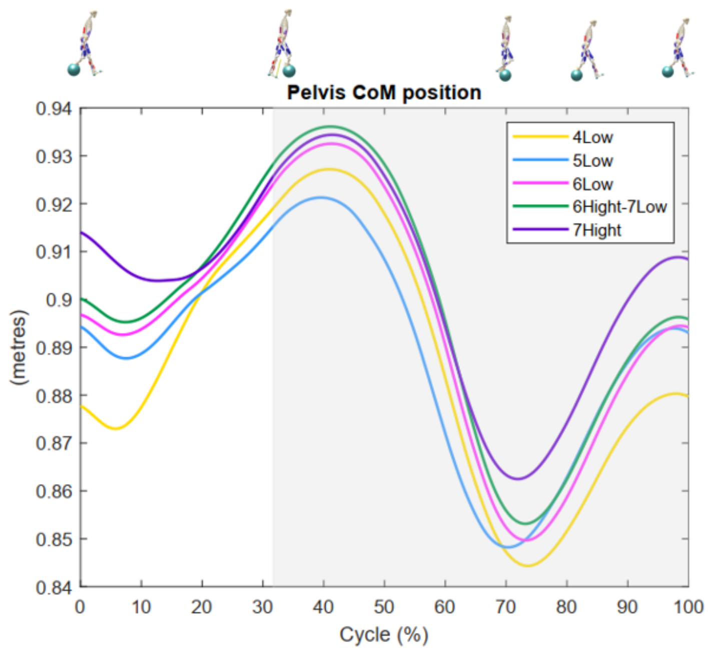

Figure B.1: Pelvis CoM position by percentage of the intact leg cycle, for the five different RSP categories.

C

Individual muscle power

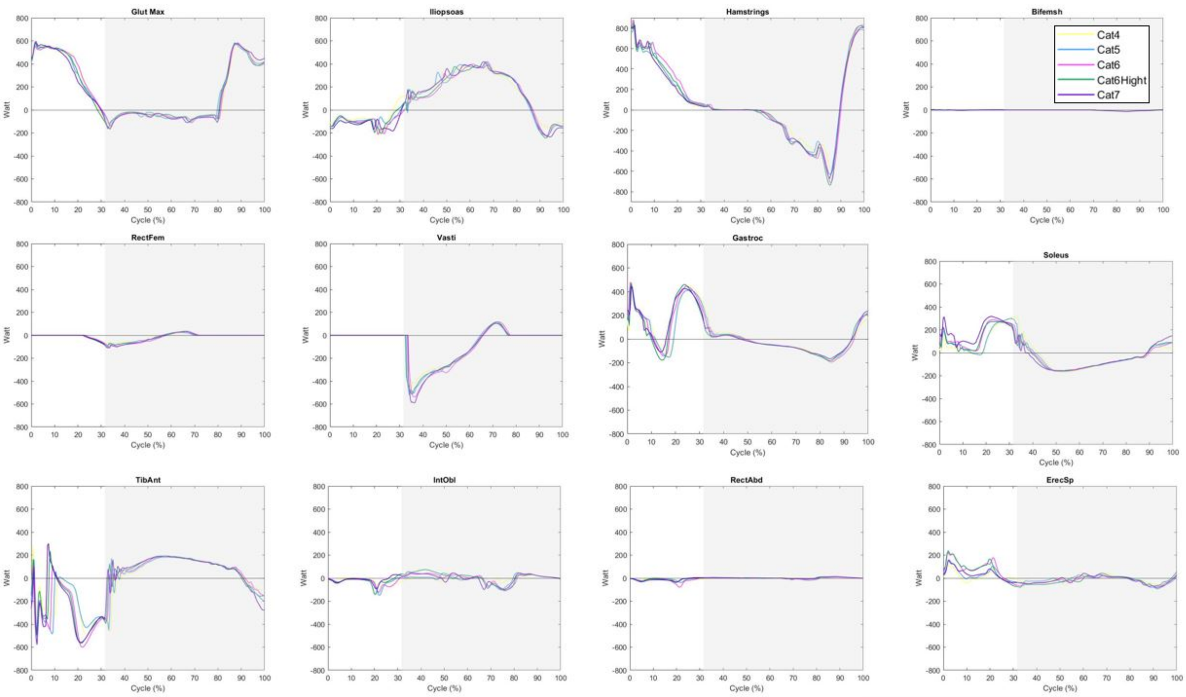

Figure C.1: Individual muscle power of the intact legs for the different stiffness categories.

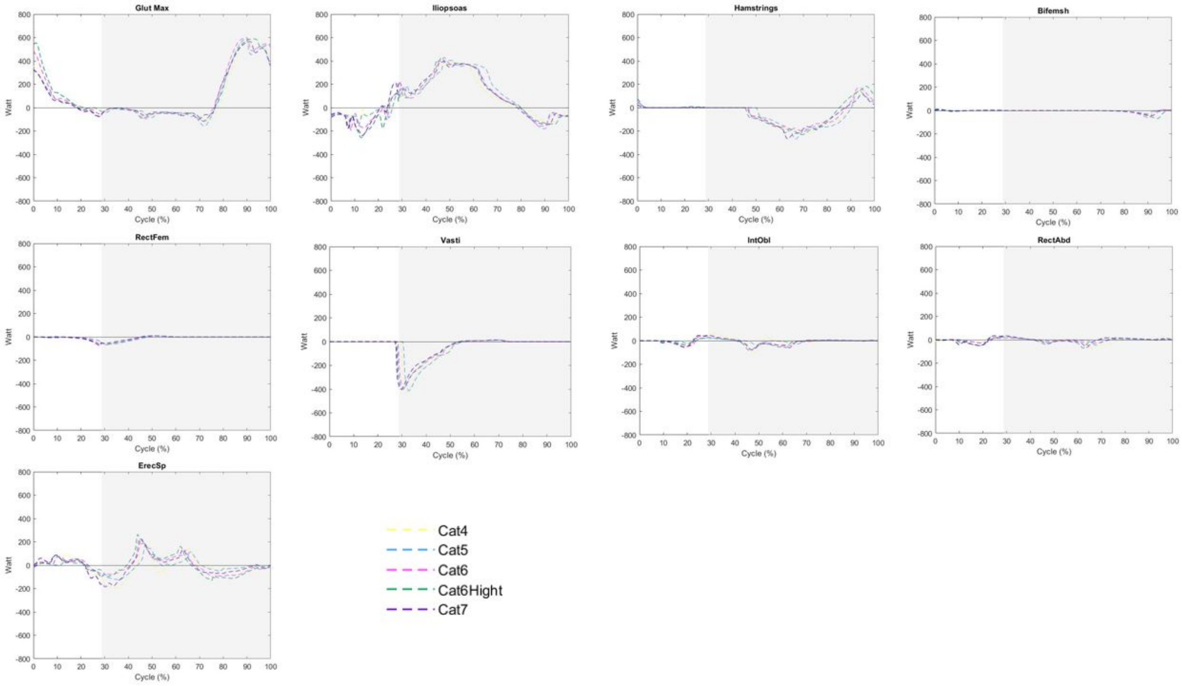

Figure C.2: Individual muscle power of the prosthetic legs for the different stiffness categories.

D

RSPs energy stored and released

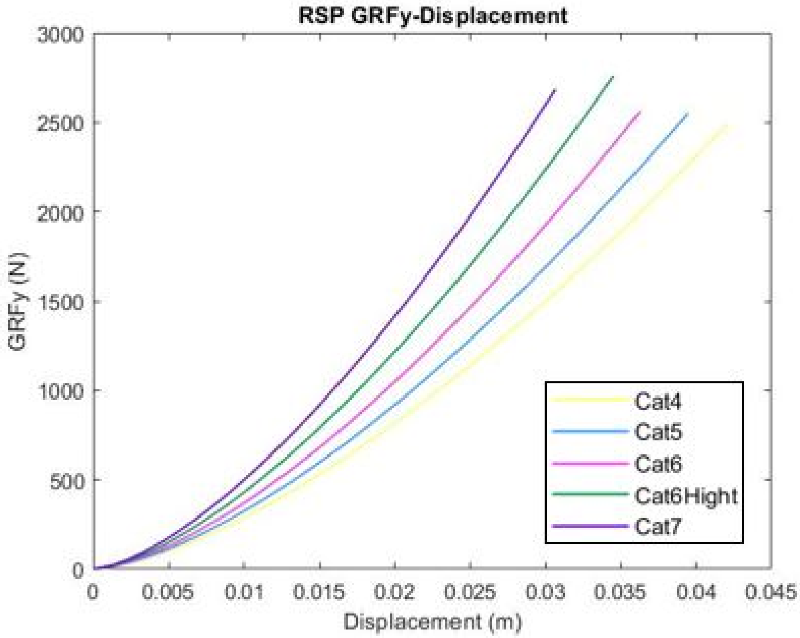

Figure D.1: GRFy-Displacement curve of each RSP during a cycle.

Stiffness Category	E stored in a cycle (J)	E returned in a cycle (J)	Hystheresis (J)	Recoil (%)
Cat4	41.09	41	0.092	99.78
Cat5	39.67	39.55	0.125	99.68
Cat6	37.55	37.44	0.118	99.69
Cat6High	38.45	38.34	0.116	99.7
Cat7	33.84	33.73	0.113	99.67

Table D.1: Energy stored, released, hysteresis and recoiled for every RSP category.

E

Muscle excitation

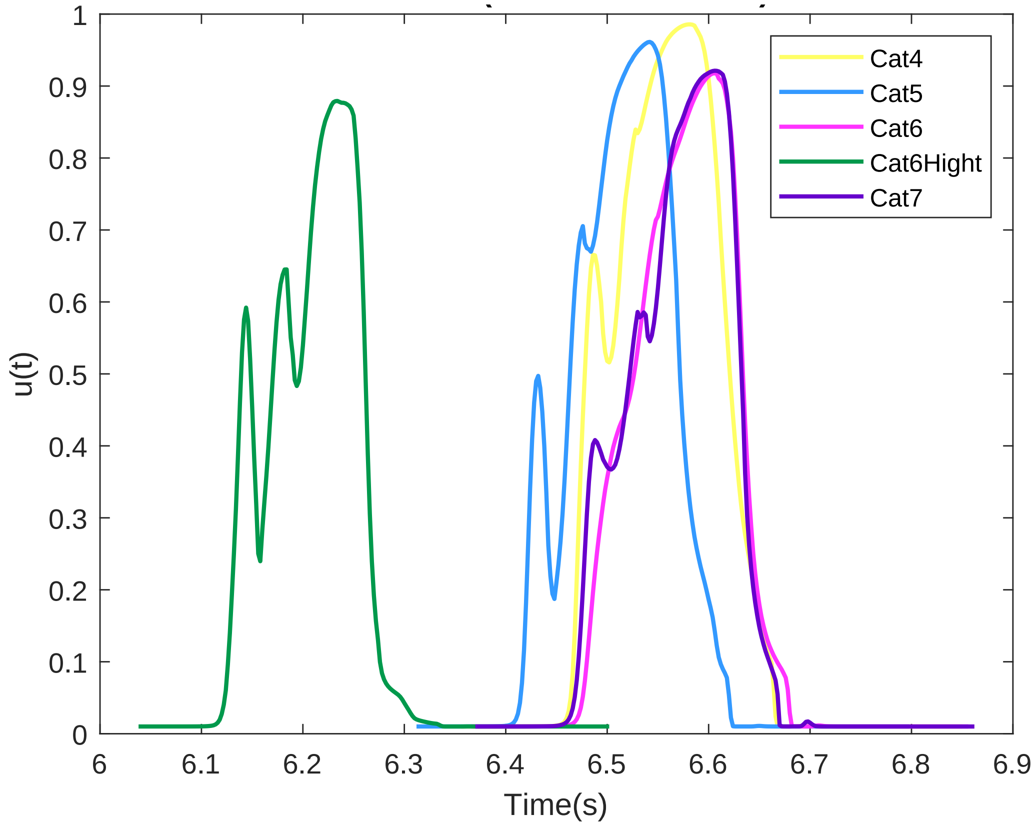

Figure E.1: In this graphs it can be seen the **excitation function of the Gluteus maximus in time**. The Cat4 and Cat5 had greater excitation peaks and the stimulus was slightly longer in time. Probably, for this reason the metabolic cost of the model was higher when wearing these two categories.

Bibliography

[1] Amputation Statistics from Ossur. `https://assets.ossur.com/library/41230`.

[2] Christopher J. Arellano and Rodger Kram. Partitioning the Metabolic Cost of Human Running: A Task-by-Task Approach. *Integrative and Comparative Biology*, 54(6):1084–1098, December 2014. ISSN 1540-7063, 1557-7023. doi: 10.1093/icb/icu033. URL `https://academic.oup.com/icb/article/54/6/1084/637436`.

[3] Brian S. Baum, Hiroaki Hobara, Yoon Hyuk Kim, and Jae Kun Shim. Amputee Locomotion: Ground Reaction Forces During Submaximal Running With Running-Specific Prostheses. *Journal of Applied Biomechanics*, 32(3):287–294, June 2016. ISSN 1065-8483, 1543-2688. doi: 10.1123/jab.2014-0290. URL `https://journals.humankinetics.com/view/journals/jab/32/3/article-p287.xml`.

[4] Brian S. Baum, Hiroaki Hobara, Kyung Koh, Hyun Joon Kwon, Ross H. Miller, and Jae Kun Shim. Amputee Locomotion: Joint Moment Adaptations to Running Speed Using Running-Specific Prostheses after Unilateral Transtibial Amputation. *American Journal of Physical Medicine & Rehabilitation*, 98(3):182–190, March 2019. ISSN 0894-9115. doi: 10.1097/PHM.0000000000000905. URL `http://Insights.ovid.com/crossref?an=00002060-201903000-00003`.

[5] Owen N Beck and Alena Grabowski. The biomechanics of the fastest sprinter withth a unilateral transtibial amputation, 2017.

[6] Owen N Beck, Paolo Taboga, and Alena M Grabowski. Characterizing the mechanical properties of running-specific prostheses. *PLoS One*, 11(12):e0168298, 2016.

[7] Arthur Jason De Luigi and Rory A. Cooper. Adaptive Sports Technology and Biomechanics: Prosthetics. *PM&R*, 6:S40–S57, August 2014. ISSN 19341482. doi: 10.1016/j.pmrj.2014.06.011. URL `http://doi.wiley.com/10.1016/j.pmrj.2014.06.011`.

[8] S. L. Delp, J. P. Loan, M. G. Hoy, F. E. Zajac, E. L. Topp, and J. M. Rosen. An interactive graphics-based model of the lower extremity to study orthopaedic surgical procedures. *IEEE Transactions on Biomedical Engineering*, 37(8):757–767, 1990. doi: 10.1109/10.102791.

[9] Thomas Geijtenbeek. Scone: Open source software for predictive simulation of biological motion. *Journal of Open Source Software*, 4(38):1421, 2019. doi: 10.21105/joss.01421. URL `https://doi.org/10.21105/joss.01421`.

[10] Lara Grobler. Characterisation of running specific prostheses and its effect on sprinting performance. page 103.

[11] Lara Grobler. *Characterisation of running specific prostheses and its effect on sprinting performance*. PhD thesis, Stellenbosch: Stellenbosch University, 2015.

[12] Lara Grobler and Wayne Derman. Sport-Specific Limb Prostheses in Para Sport. *Physical Medicine and Rehabilitation Clinics of North America*, 29(2):371–385, May 2018. ISSN 10479651. doi: 10.1016/j.pmr.2018.01.012. URL `https://linkinghub.elsevier.com/retrieve/pii/S1047965118300123`.

[13] Geoffrey G Handsfield, Craig H Meyer, Joseph M Hart, Mark F Abel, and Silvia S Blemker. Relationships of 35 lower limb muscles to height and body mass quantified using mri. *Journal of biomechanics*, 47(3):631–638, 2014.

[14] Hiroaki Hobara, Kazuyuki Kanosue, and Shuji Suzuki. Changes in muscle activity with increase in leg stiffness during hopping. *Neuroscience letters*, 418(1):55–59, 2007.

[15] Hiroaki Hobara, Brian S Baum, Hyun-Joon Kwon, Alison Linberg, Erik J Wolf, Ross H Miller, and Jae Kun Shim. Amputee locomotion: lower extremity loading using running-specific prostheses. *Gait & posture*, 39(1):386–390, 2014.

[16] Anna Lena Kleesattel, Debora Clever, Johannes Funken, Wolfgang Potthast, and Katja Mombaur. Modeling and optimal control of able-bodied and unilateral amputee running. *ISBS Proceedings Archive*, 35 (1):20, 2017.

[17] AK LaPrè, MA Price, RD Wedge, BR Umberger, and Frank C Sup IV. Approach for gait analysis in persons with limb loss including residuum and prosthesis socket dynamics. *International journal for numerical methods in biomedical engineering*, 34(4):e2936, 2018.

[18] Gavin L Moir. Biomechanics of fundamental Movements: Sprint running, 2015.

[19] Lee Nolan. Carbon fibre prostheses and running in amputees: A review. *Foot and Ankle Surgery*, 14 (3):125–129, January 2008. ISSN 12687731. doi: 10.1016/j.fas.2008.05.007. URL `https://linkinghub.elsevier.com/retrieve/pii/S1268773108000672`.

[20] Sergi Nuell, Víctor R Illera-Domínguez, Gerard Carmona, Xavier Alomar, Josep Maria Padullés, Mario Lloret, and Joan Aureli Cadefau. Hypertrophic muscle changes and sprint performance enhancement during a sprint-based training macrocycle in national-level sprinters. *European journal of sport science*, 20(6):793–802, 2020.

[21] Carmichael F Ong, Thomas Geijtenbeek, Jennifer L Hicks, and Scott L Delp. Predicting gait adaptations due to ankle plantarflexor muscle weakness and contracture using physics-based musculoskeletal simulations. *PLoS computational biology*, 15(10):e1006993, 2019.

[22] Laura M Oudenhoven, Judith M Boes, Laura Hak, Gert S Faber, and Han Houdijk. Regulation of step frequency in transtibial amputee endurance athletes using a running-specific prosthesis. *Journal of biomechanics*, 51:42–48, 2017.

[23] Antonio Pappalardo, Abdulrahman Albakri, Chao Liu, Luca Bascetta, Elena De Momi, and Philippe Poignet. Hunt–crossley model based force control for minimally invasive robotic surgery. *Biomedical Signal Processing and Control*, 29:31–43, 2016.

[24] Apoorva Rajagopal, Christopher L Dembia, Matthew S DeMers, Denny D Delp, Jennifer L Hicks, and Scott L Delp. Full-body musculoskeletal model for muscle-driven simulation of human gait. *IEEE transactions on biomedical engineering*, 63(10):2068–2079, 2016.

[25] Stacey M Rigney, Anne Simmons, and Lauren Kark. A prosthesis-specific multi-link segment model of lower-limb amputee sprinting. *Journal of biomechanics*, 49(14):3185–3193, 2016.

[26] Lauren A Sepp, Erika Nelson-Wong, Brian S Baum, and Anne K Silverman. Running-specific prostheses reduce lower-limb muscle activity compared to daily-use prostheses in people with unilateral transtibial amputations. *Journal of Electromyography and Kinesiology*, 55:102462, 2020.

[27] André Seyfarth and Christian Schumacher. Teaching locomotion biomechanics: from concepts to applications. *Eur. J. Phys.*, 40(2):024004, March 2019. ISSN 0143-0807, 1361-6404. doi: 10.1088/1361-6404/aaf136. URL `http://stacks.iop.org/0143-0807/40/i=2/a=024004?key=crossref.8dc7e026dd0bdcf843d73c63a383a462`.

[28] Siobhan C. Strike, Daniela Arcone, and Michael Orendurff. Running at submaximal speeds, the role of the intact and prosthetic limbs for trans-tibial amputees. *Gait & Posture*, 62:327–332, May 2018. ISSN 09666362. doi: 10.1016/j.gaitpost.2018.03.030. URL `https://linkinghub.elsevier.com/retrieve/pii/S0966636218302297`.

[29] Thomas K Uchida, Jennifer L Hicks, Christopher L Dembia, and Scott L Delp. Stretching your energetic budget: how tendon compliance affects the metabolic cost of running. *PloS one*, 11(3):e0150378, 2016.

[30] E Van der Kruk, FCT van der Helm, HEJ Veeger, and AL Schwab. Power in sports: a literature review on the application, assumptions, and terminology of mechanical power in sport research. *Journal of biomechanics*, 79:1–14, 2018.

[31] Peter G. Weyand, Deborah B. Sternlight, Matthew J. Bellizzi, and Seth Wright. Faster top running speeds are achieved with greater ground forces not more rapid leg movements. *Journal of Applied Physiology*, 89(5):1991–1999, November 2000. ISSN 8750-7587, 1522-1601. doi: 10.1152/jappl.2000.89.5.1991. URL https://www.physiology.org/doi/10.1152/jappl.2000.89.5.1991.